Cell

An Integrated Approach Reveals Regulatory Controls on Bacterial Translation Elongation

Arvind R. Subramaniam,[1,2,*] Brian M. Zid,[1,2] and Erin K. O'Shea[1,2,3,4,*]
[1]Faculty of Arts and Sciences Center for Systems Biology
[2]Department of Molecular and Cellular Biology
[3]Department of Chemistry and Chemical Biology
[4]Howard Hughes Medical Institute
Harvard University, Cambridge, MA 02138, USA
*Correspondence: asubram@fas.harvard.edu (A.R.S.), erin_oshea@harvard.edu (E.K.O.)
http://dx.doi.org/10.1016/j.cell.2014.10.043

SUMMARY

Ribosomes elongate at a nonuniform rate during translation. Theoretical models and experiments disagree on the in vivo determinants of elongation rate and the mechanism by which elongation rate affects protein levels. To resolve this conflict, we measured transcriptome-wide ribosome occupancy under multiple conditions and used it to formulate a whole-cell model of translation in *E. coli*. Our model predicts that elongation rates at most codons during nutrient-rich growth are not limited by the intracellular concentrations of aminoacyl-tRNAs. However, elongation pausing during starvation for single amino acids is highly sensitive to the kinetics of tRNA aminoacylation. We further show that translation abortion upon pausing accounts for the observed ribosome occupancy along mRNAs during starvation. Abortion reduces global protein synthesis, but it enhances the translation of a subset of mRNAs. These results suggest a regulatory role for aminoacylation and abortion during stress, and our study provides an experimentally constrained framework for modeling translation.

INTRODUCTION

Protein synthesis begins with initiation by ribosomes on an mRNA and is followed by a sequence of elongation steps during which amino acids are added to the growing polypeptide chain. Initiation is the rate-limiting step for the translation of most mRNAs during nutrient-rich growth (Jacques and Dreyfus, 1990). However, stressful perturbations such as amino acid starvation or transgene overexpression can decrease the elongation rate of ribosomes and affect protein levels (Subramaniam et al., 2013a; Varenne et al., 1984; Welch et al., 2009). Biophysical modeling of translation can be used to infer the quantitative effect of these stressful perturbations on initiation rate, elongation rate, and the expression level of proteins (Shah et al., 2013). More generally, modeling integrates our biochemical knowledge of translation and thus enables identification of novel regulatory processes when incorporation of known mechanisms is insufficient to recapitulate experimental measurements.

Biophysical modeling of translation has been greatly aided by the development of ribosome profiling, which involves deep sequencing of ribosome-protected mRNA fragments to measure ribosome occupancy on mRNAs (Ingolia et al., 2009). Ribosome profiling has also produced surprising results that challenge two central assumptions in current theoretical models of translation. First, theoretical models assume that elongation rates at codons are directly proportional to the intracellular concentration of cognate aminoacyl-tRNAs (aa-tRNAs) during nutrient-rich growth (Shah et al., 2013; Tuller et al., 2010). However, this assumption is not supported by ribosome profiling—although concentrations of different tRNAs vary over greater than a 10-fold range in bacteria and yeast (Dong et al., 1996; Tuller et al., 2010), the measured ribosome occupancy at codons varies less than 2-fold in these organisms during nutrient-rich growth (Li et al., 2012; Qian et al., 2012). Differential aminoacylation of tRNAs is also unlikely to underlie this discrepancy, as most tRNA species are >70% aminoacylated during nutrient-rich growth (Yegian et al., 1966). Second, most models assume that a decrease in ribosome elongation rate on an mRNA affects the level of the corresponding protein by causing a traffic jam of trailing ribosomes (Shah et al., 2013; Zhang et al., 1994). However, except for a few atypical mRNAs (Guydosh and Green, 2014; Li et al., 2012), traffic jams at ribosome pause sites have not been observed in vivo, and the effect of ribosome traffic jams on protein level remains unclear. Together, these results suggest that current theoretical models do not include the full set of mechanistic ingredients that is necessary for accurate modeling of in vivo translation, especially as it pertains to the elongation stage.

To identify mechanistic features of the elongation stage that enable accurate biophysical modeling of translation, we combined transcriptome-scale and reporter-based experiments with whole-cell computational modeling. This approach enabled us to decipher the contribution of various molecular processes to the elongation rate of ribosomes and the synthesis rate of proteins. We found that the differences in the intracellular concentration of tRNAs and the occurrence of ribosome traffic jams at pause sites, both of which have been key ingredients in previous theoretical models (Shah et al., 2013; Tuller

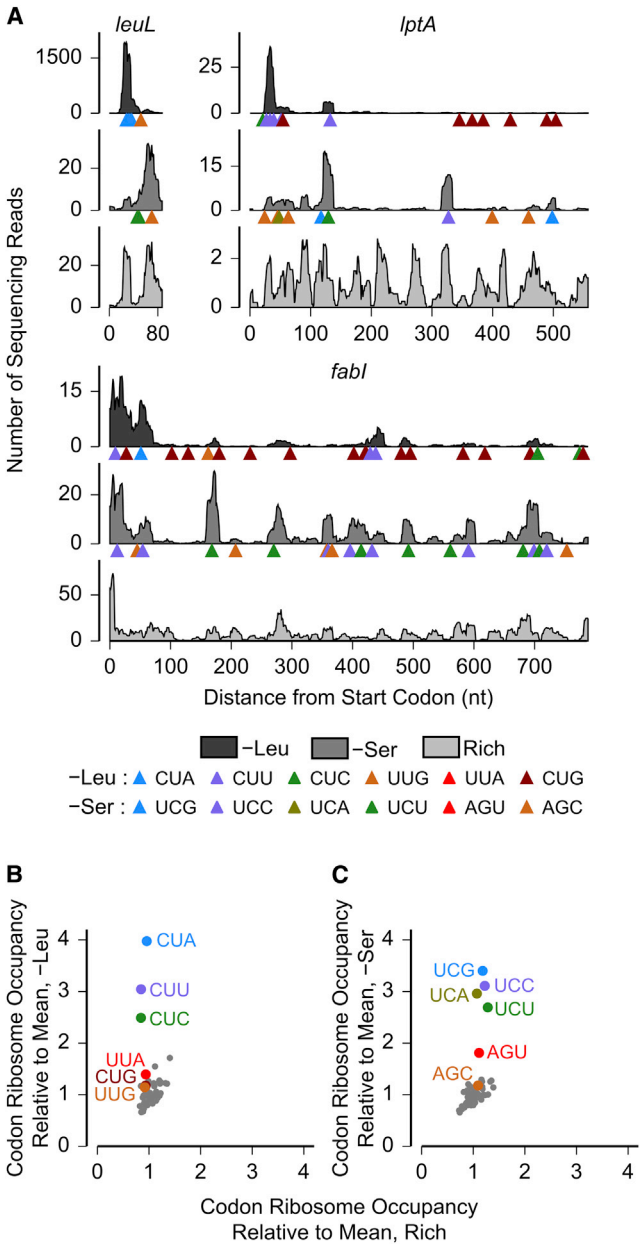

Figure 1. Changes in Ribosome Occupancy upon Starvation for Single Amino Acids

(A) Measured ribosome occupancy along three *E. coli* genes: *leuL*, *lptA*, and *fabI* during leucine starvation (–Leu), serine starvation (–Ser), and amino-acid-rich growth (Rich). The horizontal axis extends from the start codon to the stop codon for each gene. Triangles indicate the positions of leucine (serine) codons along the coding sequence in the leucine (serine) starvation case.

(B and C) Measured ribosome occupancy at the 61 sense codons averaged across the transcriptome. Start and stop codons are not shown. Standard errors of mean are smaller than data markers.

See also Figure S1.

et al., 2010), are insufficient to predict the measured ribosome occupancy in our experiments. We find that the molecular process of aminoacylation has a critical role in protein synthesis through modulation of ribosome elongation rates during stress. Further, we find that premature termination of translation before the synthesis of full-length proteins (henceforth referred to as translation abortion) determines both the ribosome occupancy along mRNAs and protein expression during stress. More generally, our work illustrates the usefulness of integrating deep-sequencing experimental methods such as ribosome profiling together with quantitative whole-cell modeling to reveal the experimentally relevant regimes of the a priori large parameter space in biophysical models of complex cellular processes.

RESULTS

Changes in Ribosome Occupancy upon Starvation for Single Amino Acids

We previously found that, during starvation for single amino acids in *E. coli*, the presence of certain codons cognate to the limiting amino acid can decrease the protein synthesis rate by up to 100-fold (Subramaniam et al., 2013a). Starvation for single amino acids decreases the concentration of the cognate aminoacyl (aa) tRNAs (Dittmar et al., 2005; Sørensen, 2001; Sørensen et al., 2005), thus decreasing the elongation rate of ribosomes at cognate codons. Based on these observations, we used single amino acid starvation as an experimental condition to develop constraints for biophysical models of protein synthesis in an elongation-limited regime of translation.

To characterize the effect of amino acid starvation on translation, we performed ribosome profiling in *E. coli* after 30 min of starvation for each of two amino acids: leucine and serine. For comparison with an initiation-limited regime of translation, we also performed ribosome profiling on cells grown in rich-defined medium with all 20 amino acids. The distribution of ribosome footprints along mRNAs was highly variable during nutrient-rich growth (Figure 1A), consistent with earlier observations (Oh et al., 2011). Starvation for either leucine or serine caused a pronounced change in the distribution of ribosome footprints along individual mRNAs (Figure 1A). Consistent with previous observations (Li et al., 2012), the transcriptome-averaged ribosome occupancy differed less than 2-fold across the 61 codons during nutrient-rich growth (Figures 1B and 1C, horizontal axis) and did not systematically vary with tRNA abundance (Figure S1A available online). Upon leucine or serine starvation, the average ribosome occupancy increased at leucine and serine codons, respectively, but this increase was not uniform (Figures 1B and 1C, vertical axis). The three leucine codons CUA, CUC, and CUU had 2.5- to 4-fold higher ribosome occupancy than the average during leucine starvation, whereas the ribosome occupancy at the remaining three leucine codons CUG, UUA, and UUG was comparable to that of noncognate codons. Similarly, ribosome occupancy at the four serine codons UCA, UCC, UCG, and UCU was markedly higher than at the two serine codons AGC and AGU during serine starvation. We attributed the increase in ribosome occupancy at leucine and serine codons to a decrease in the ribosome elongation rate, as we did not observe an increase in total mRNA density at these codons upon leucine or serine starvation (Figures S1B and S1C).

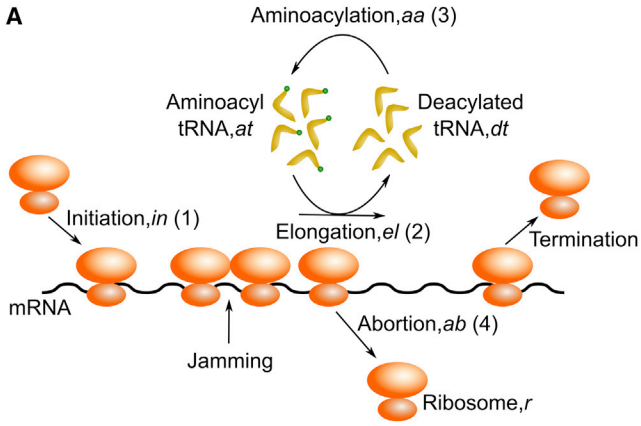

B

$$R_p^{in} = k_p^{in} n^r \quad (1)$$

$$R_a^{el} = \begin{cases} 1/\left[\tau_0 + \left(\sum_i k_{ia}^{el} w_{ia} n_i^{at}\right)^{-1}\right] & \text{if not jammed} \\ 0 & \text{if jammed} \end{cases} \quad (2)$$

$$R_i^{aa} = k_i^{aa} n_i^{dt} \quad (3)$$

$$R_a^{ab} = \begin{cases} k^{ab} & \text{if } R_a^{el} < R_{threshold}^{el} \\ 0 & \text{if } R_a^{el} > R_{threshold}^{el} \text{ or if jammed} \end{cases} \quad (4)$$

Figure 2. A Transcriptome-Scale Biophysical Model of Translation

(A) Schematic of the four cellular processes modeled (initiation, elongation, aminoacylation, abortion) and the molecular species considered in the biophysical model.

(B) Reaction rates, R_i, for the cellular processes shown in (A). The superscripts following R_i refer to the abbreviations for the cellular processes in (A). Subscript indices are used for distinct molecular species of the same kind (mRNA – p, tRNA – i, codon – a). The intracellular concentrations of molecular species and the values for rate constants in our whole-cell simulation are in Table S1.

See also Data S1.

A Transcriptome-Scale Biophysical Model of Translation in *E. coli*

To systematically evaluate the consistency of different biophysical models with our measurements of ribosome occupancy, we formulated a generalized kinetic model of protein synthesis in *E. coli* that accounted for four different molecular processes that we found to play a critical role in determining ribosome occupancy and protein expression: initiation, elongation, aminoacylation, and abortion (Figure 2A). Other molecular processes that are not expected to limit protein synthesis rate under the conditions of our study, such as termination at stop codons and ribosome recycling, were assumed to be instantaneous (rates set to infinity) for the sake of simplicity.

The core features of our biophysical model of protein synthesis are summarized by the kinetic rate equations for the four molecular processes (Figure 2B). The full list of parameter values used in our biophysical model is given in Table S1. We implemented our model as a continuous-time, discrete-state process at the whole-cell level for *E. coli* by adapting the source code from a recent computational study in yeast (Shah et al., 2013). During balanced nutrient-rich growth, the availability of free ribosomes for initiation is rate limiting for protein synthesis (Vind et al., 1993). We modeled this empirical observation by taking the initiation rate R^{in} to be proportional to n^r, the number of free ribosomes in the cell (Equation 1 in Figure 2B). The initiation rate constant k_p^{in} for each mRNA species p was estimated from our ribosome profiling measurements and the macromolecular composition and synthesis rates that have been measured with high accuracy in *E. coli* (Bremer and Dennis, 2008) (Extended Experimental Procedures).

Intraribosomal Events Limit the Rate of Elongation during Nutrient-Rich Growth

The elongation cycle is a multistep process that begins with the delivery of the aa-tRNA (in ternary complex with Ef-Tu and GTP) to the ribosome. This step is followed by a series of intraribosomal events that include kinetic proofreading, peptidyl transfer, and translocation of the ribosome to the next codon (Wintermeyer et al., 2004). We considered a minimal model of elongation (Elf et al., 2003) that is composed of two effective steps (Equation 2 in Figure 2B). The first step accounts for the arrival of cognate aa-tRNAs at the ribosome, and its rate is proportional to the intracellular concentration of aa-tRNA, n^{at}. The proportionality factor k^{el} is the second-order rate constant (k_{cat}/K_M) for association between the ribosome and the aa-tRNA. The second step accounts for all intraribosomal events that follow the arrival of the cognate aa-tRNA at the ribosome, and the cumulative rate of these events does not depend on the intracellular concentration of aa-tRNA. For simplicity, we set the total rate of this second step to a uniform value $1/\tau_0$ for all codons. Finally, when translocation is prevented by the presence of a leading ribosome (henceforth referred to as jamming), the elongation rate is set to zero in our model.

If τ_0 (the rate constant describing all intraribosomal events following arrival of the aa-tRNA) has the same value for all codons, the experimental observation that ribosome occupancies at codons do not vary inversely with the corresponding tRNA concentrations during nutrient-rich growth (Figure S1A) now implies a straightforward mechanistic constraint in our model—that the rate of intraribosomal events limits the overall rate of ribosome elongation under these conditions, i.e., $\tau_0 >> 1/k^{el}n^{at}$ in Equation 2 of Figure 2B. Together, with the measured average elongation rate of ribosomes of ~20 codons per second (Bremer and Dennis, 2008), we can then infer that $\tau_0 \approx 0.05$ s. In the more general case in which τ_0 is not uniform for all codons, most of the codons still need to have $\tau_0 \gg 1/k^{el}n^{at}$ to recapitulate the observed lack of (inverse) proportionality between ribosome occupancy and tRNA concentration. Our conclusion that $\tau_0 >> 1/k^{el}n^{at}$, based solely on ribosome occupancy measurements, is also consistent with the typical in vitro value of $k^{el} = 2 \times 10^7\ M^{-1}s^{-1}$ (Bilgin and Ehrenberg, 1994; Pavlov and Ehrenberg, 1996) and the in vivo concentrations of tRNAs (n^{at}) during nutrient-rich growth (Bremer and Dennis, 2008; Dong et al., 1996) (Data S1). Using these values of k^{el} and n^{at}, the median value of $1/k^{el}n^{at}$ for the 61 sense codons is 0.0036 s, and all codons had $1/k^{el}n^{at} < 0.013$ s ($\ll \tau_0 \approx 0.05$ s).

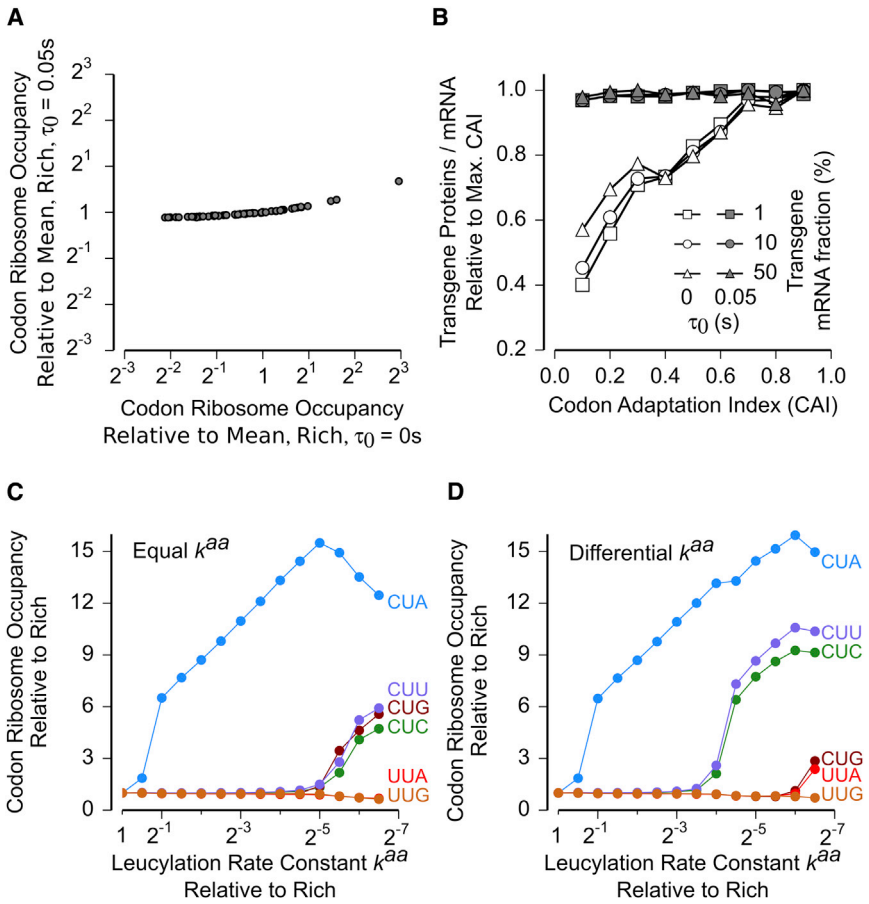

Figure 3. Elongation and Aminoacylation Kinetics Determine Ribosome Occupancy at Codons

(A) Mean ribosome occupancy at the 61 sense codons averaged across the transcriptome during nutrient-rich growth calculated from whole-cell model. Simulations were run with the time for intraribosomal events at a single codon, τ_0, set to either 0 s (horizontal) or 0.05 s (vertical). The value of k^{el} was chosen such that the mean elongation rate of ribosomes R^{el} was approximately equal to the experimentally measured value of 20 s^{-1} in both cases.

(B) Amount of transgene proteins produced per mRNA upon overexpression during nutrient-rich growth calculated from whole-cell model as a function of codon adaptation index (CAI) and the transgene fraction. All data points corresponding to a single transgene mRNA fraction were normalized by the data point at CAI = 0.9.

(C and D) Mean ribosome occupancy at the six leucine codons as a function of leucylation rate constant calculated from whole-cell model. The leucylation rate constants of the five leucine tRNA isoacceptors were set either equal (C) or different (D). In the differential case (D), the leucylation rate constants were in the proportion 1.5: 0.5: 1: 0.5: 0.5 (Leu1 through Leu5).

See also Figure S2.

To test the consistency of our whole-cell model with ribosome profiling measurements, we simulated our model with the above-constrained rate constants for elongation. With τ_0 = 0.05 s and k^{el} = 2 × 10^7 $M^{-1}s^{-1}$, we observed less than 2-fold variation (SD/mean = 10%) in ribosome occupancy across the 61 codons (Figure 3A, vertical axis). By contrast, when we set the timescale of intraribosomal events to be zero (τ_0 = 0 s), as assumed in previous work (Shah et al., 2013; Tuller et al., 2010), ribosome occupancy varied 34-fold (SD/mean = 105%) across the 61 codons (Figure 3A, horizontal axis), even though for both values of τ_0 (0.05 and 0 s), the average elongation rate (R^{el}) was ~20 codons s^{-1}. Thus, we conclude that ribosome occupancy at codons during nutrient-rich growth of *E. coli*, as measured using ribosome profiling, is consistent with a model in which intraribosomal events, rather than the arrival of aa-tRNA to the ribosome A site, are the slowest steps in the elongation cycle for most codons.

Highly expressed genes in *E. coli*, such as those coding for the translation machinery, display a characteristic codon bias (called the major codon bias) toward codons that are decoded by tRNA isoacceptors with high intracellular concentration (Andersson and Kurland, 1990). Motivated by this observation, biophysical models often predict that optimizing the codon usage of an overexpressed transgene by enriching for codons decoded by abundant tRNA isoacceptors can significantly improve the yield of its protein (Shah et al., 2013; Zhang et al., 1994). Because this question is of significant interest in biotechnological applications (Gustafsson et al., 2004), we re-examined it in the light of our conclusion that intraribosomal events, rather than the arrival of aa-tRNA, limit the rate of elongation during nutrient-rich growth.

We simulated the expression of three transgenes at different fractions of the cellular transcriptome and with various codon bias (Extended Experimental Procedures and Data S1). When we assumed that the elongation rate at codons is proportional to the concentration of aa-tRNAs (by setting τ_0 = 0 s in Equation 2 of Figure 2B), we found that increasing codon bias can improve protein expression from the transgenes by >2-fold (Figure 3B, open markers). However, this effect of codon bias was essentially absent when elongation rates at codons were limited by intraribosomal events (Figure 3B, filled markers). We observed a similar effect of intraribosomal events when we simulated a model for yeast translation (Shah et al., 2013) (Figure S2A). The lack of effect of codon bias on transgene overexpression is consistent with measurements using synthetic gene libraries in *E. coli*, which detected little correlation between yield of overexpressed proteins and the codon adaptation index (Kudla et al., 2009; Welch et al., 2009). Thus, based on the elongation kinetics inferred from ribosome profiling, we suggest that the major codon bias is not a significant determinant of protein yield during transgene overexpression in *E. coli*.

Differential Aminoacylation Determines the Specificity of Elongation Pausing

Having formulated our biophysical model during nutrient-rich growth when initiation is rate limiting for translation, we sought

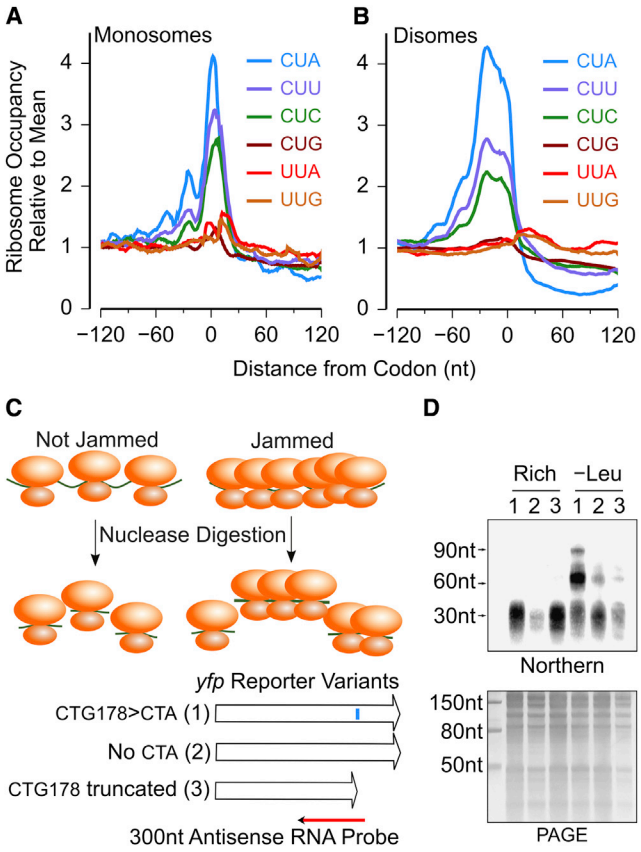

Figure 4. Ribosome Traffic Jams at Ribosome Pause Sites

(A) Measured monosome occupancy from −120 nt to +120 nt around the six leucine codons during leucine starvation. The monosome occupancy was averaged across all occurrences of each codon in the transcriptome.

(B) Measured disome occupancy from −120 nt to +120 nt around the six leucine codons during leucine starvation. The disome occupancy was averaged across all occurrences of each codon in the transcriptome.

(C) Nuclease footprinting assay for detecting ribosome traffic jams on *yfp* reporter mRNAs. The blue vertical bar along the first variant indicates the location of the CTG200 > CTA substitution. Northern blotting was performed using a ^{32}P-labeled antisense RNA complementary to the 300 nt mRNA region from −250 nt to +50 nt of the CTG200 > CTA substitution.

(D) (Top) Northern blot of nuclease-digested polysomes for the three *yfp* variants. (Bottom) Polyacrylamide gel corresponding to the northern blot. Numbers above individual lanes correspond to the three *yfp* variants in (C). The size markers on the left of the northern blot were inferred by aligning it to the polyacrylamide gel image. The arrows at 30, 60, and 90 nt indicate the approximate locations of monosomes, disomes, and trisomes, respectively.

See also Figure S3.

to test our model in an elongation-limited regime during starvation for single amino acids. To simulate starvation for a single amino acid, we reduced the aminoacylation rate constant of the corresponding tRNA isoacceptors (k^{aa} in Equation 3 in Figure 2B) while keeping all other parameters identical to those during nutrient-rich growth. Reducing the leucylation or the serylation rate constant caused a nonuniform increase in ribosome occupancy at leucine and serine codons, respectively (Figures 3C and S2B). However, the hierarchy predicted by the model significantly deviated from the measured hierarchy among these codons during both leucine and serine starvation (Figures 1B and 1C).

The discrepancy between model and experiments in the hierarchy of ribosome occupancy at codons during starvation could arise from two sources. One possibility is that the uniform rate constants for codon-tRNA interaction (k^{el}) could differ between tRNA isoacceptors, as we used only average estimates in our model. However, when we replaced the average estimates with in vitro measurements of k^{el}, which vary over a 3-fold range for the leucine family (Sørensen et al., 2005), it had little effect on the predicted hierarchy of ribosome occupancy at codons (Figure S2C). A second explanation for the above discrepancy is that the rate constants for aminoacylation (k^{aa}) might be unequal between the different tRNA isoaccceptors. Indeed, when we allowed the aminoacylation rate constants for tRNA isoacceptors to differ over a 3-fold range (Figure S2D), the model could largely recapitulate the experimentally measured hierarchy among codons during starvation (Figures 3D and S2E). Our modeling of differential aminoacylation kinetics is consistent with previous in vitro measurements, which found that tRNA isoacceptors could differ 2- to 20-fold in their aminoacylation rate constants (Fender et al., 2004; Harris and Marashi, 1980; Myers et al., 1971).

Accounting for aminoacylation itself has a critical effect on protein expression during amino acid starvation. A recent modeling study arrived at the conclusion that protein expression can be rescued during amino acid starvation by reducing the number of ribosomes in the cell (Shah et al., 2013). This conclusion was based on lowering the total number of tRNAs to simulate amino acid starvation without considering aminoacylation (Figure S2F). However, there is little evidence that the total concentration of tRNAs significantly changes upon amino acid starvation, whereas the canonical effect of amino acid starvation is the reduction in aminoacyl-tRNA concentration due to lower aminoacylation rate (Dittmar et al., 2005; Sørensen, 2001; Sørensen et al., 2005). When we simulated starvation by reducing the levels of aminoacyl-tRNA rather than that of total tRNA using the model of Shah et al., (2013), we did not observe rescue of protein expression upon decreasing the number of ribosomes (Figure S2G). Thus, accounting for aminoacylation qualitatively alters the prediction from biophysical models of translation in the elongation-limited regime of amino acid starvation.

Ribosome Traffic Jams at Ribosome Pause Sites during Amino Acid Starvation

Single mRNAs are often simultaneously translated by several ribosomes. As a result, if ribosomes pause for a sufficiently long duration during elongation, a traffic jam of trailing ribosomes can occur in the 5′ region of the ribosome pause site. To detect traffic jams in our ribosome profiling measurement, we calculated the average ribosome occupancy across the transcriptome in the 120 nt region on either side of the leucine codons during leucine starvation (Figure 4A). We observed an increase in ribosome occupancy at three of the leucine codons—CUA, CUC, and CUU—which is consistent with ribosomes pausing at these codons during elongation. In addition, we observed smaller peaks in ribosome density centered approximately −28 nt and −56 nt upstream of these three codons (Figure 4A). These peaks are consistent with a traffic jam of one and two ribosomes behind

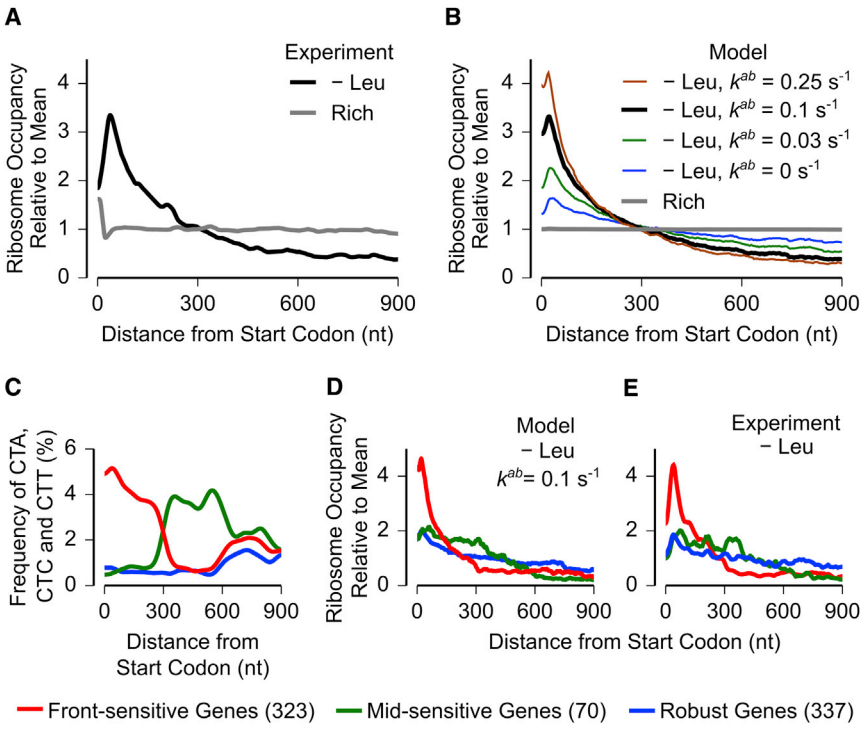

Figure 5. Translation Abortion Determines the Distribution of Ribosomes along mRNAs during Amino Acid Starvation

(A) Measured ribosome occupancy along mRNAs averaged across the transcriptome (1,518 genes).

(B) Ribosome occupancy along mRNAs averaged across the transcriptome (1,518 genes) calculated from the whole-cell model. The abortion rate constant k^{ab} was varied. Leucine starvation was modeled as a constant 100-fold reduction in the leucylation rate constant, $k^{aa,\,Leu}$.

(C) Codon frequency of the three leucine codons—CTA, CTC, and CTT—in three sets of genes (red, green, blue) with different intragenic distributions of these codons. The number of genes in each class is shown between parentheses in the legend. The codon frequency distribution was smoothed using a Gaussian window of 30 nt width.

(D) Ribosome occupancy averaged across the three sets of genes during leucine starvation calculated from the whole-cell model.

(E) Measured ribosome occupancy averaged across the three sets of genes during leucine starvation.

Ribosome occupancy profiles in all panels were smoothed using a sliding window of 30 nt. Each ribosome occupancy profile was normalized to have a mean value of 1. See also Figure S4.

the paused ribosome. We observed similar but smaller peaks at −28 nt for four of the six serine codons during serine starvation (Figure S3A). Notably, we did not observe smaller peaks upstream of Shine-Dalgarno-like codons, which also cause an increase in ribosome occupancy during nutrient-rich growth (Li et al., 2012) (Figure S3B).

Previous work has shown that nuclease treatment of polysomes with ribosome traffic jams can result in longer mRNA footprints that are protected by multiple ribosomes (Guydosh and Green, 2014; Wolin and Walter, 1988). To test whether longer mRNA footprints occur during amino acid starvation in *E. coli*, we measured the size of nuclease-protected mRNA fragments using three yellow fluorescent protein (*yfp*) reporter variants (Figure 4C). We observed a ~30 nt fragment corresponding to the monosome for all *yfp* variants both during rich growth and during leucine starvation (Figure 4D). In addition, we observed a prominent ~60 nt fragment and a weaker ~90 nt fragment in the *yfp* variant with the CUA codon during leucine starvation. These longer fragments were either faint or absent in the control variants without CUA codons and during nutrient-rich growth, which is consistent with a traffic jam of multiple ribosomes caused by pausing of ribosomes at the CUA codon during leucine starvation. These results also suggest that the standard ribosome profiling method, in which only monosome-protected fragments are sequenced, underestimates the actual in vivo magnitude of ribosome occupancy 5′ to the pause site in the presence of ribosome traffic jams. Deep sequencing of longer mRNA fragments (50–80 nt) that were protected by two ribosomes (disomes) from nuclease digestion revealed an increase in average disome occupancy up to 90 nt upstream of CUA codons during leucine starvation (Figure 4B), which is consistent with a traffic jam of between two to three ribosomes behind the paused ribosome. The length of this region with increased footprint density was similar to that obtained using the standard ribosome profiling method in which only short (~30 nt) monosome-protected mRNA fragments were sequenced (Figure 4A), which suggests that both the paused, leading ribosome as well as the jammed, trailing ribosomes have an equal likelihood of occurring either as monosomes or as disomes upon nuclease treatment.

Translation Abortion Determines the Distribution of Ribosomes along mRNAs during Amino Acid Starvation

The strong ribosome pausing that we observed during starvation for single amino acids enabled us to test whether the measured ribosome occupancy along mRNAs is quantitatively consistent with a biophysical model of ribosome traffic jams. During nutrient-rich growth, except for a peak at the start codon, ribosome occupancy was uniformly distributed across the entire length of the mRNA (Figure 5A, gray line), which is similar to previous observations (Oh et al., 2011). By contrast, during starvation for leucine, the distribution of ribosome occupancy was highly nonuniform, varying over a 10-fold range within the first 900 nt (Figure 5A, black line). Ribosome occupancy increased sharply to a maximum at around 30 nt from the start codon and then decreased toward the 3′ end of the mRNA. Starvation for serine produced a similar but less skewed distribution of ribosome occupancy along mRNAs (Figure S4A). By comparison, the distribution of total mRNA density was not significantly skewed during leucine starvation (Figure S4B).

We then used the distribution of measured ribosome occupancy along mRNAs to evaluate our biophysical model of translation. Our model reproduced the uniform distribution of measured ribosome occupancy during nutrient-rich growth (Figure 5B, gray line), which is consistent with initiation being rate limiting for translation under these conditions (Li et al., 2014). However, when we simulated leucine starvation by a 100-fold reduction in the leucylation rate constant, a model that included only ribosome traffic jams predicted a more uniform distribution of ribosome occupancy than the one observed experimentally (Figure 5B, blue line, compared to black line in Figure 5A). This disagreement between the model and our measurements could not be offset by varying the leucylation rate, the only remaining free parameter in our model, over a 1,000-fold range (Figure S4C) and was also observed for serine starvation (Figure S4D).

The discrepancy in the distribution of ribosome occupancy between ribosome profiling measurements and our model that included only ribosome traffic jams led us to consider other molecular processes that occur in response to ribosome pausing. Translation abortion is a widespread mechanism of ribosome rescue that has been observed in both bacteria and eukaryotes in response to ribosome pausing (Shoemaker and Green, 2012). Inactivation of translation abortion factors can decrease the growth rate of cells during stressful perturbations (Keiler and Feaga, 2014), indicating the importance of abortion during stress. We modeled translation abortion (Equation 4 in Figure 2B) as occurring at a constant rate k^{ab} whenever the elongation rate of ribosomes falls below a threshold, $R^{el}{}_{threshold}$. This threshold elongation rate was set below the elongation rate of all codons under nutrient-rich growth to account for the experimental observation that abortion is generally selective for paused ribosomes (Moore and Sauer, 2005). In our model, increasing the rate of translation abortion (k^{ab}) produced higher ribosome occupancy at the 5′ end of mRNAs during starvation (Figures 5B and S4D). An in vivo abortion rate (k^{ab}) of ~0.1 s^{-1} in our model predicted an average distribution of ribosome occupancy that matched the experimentally observed distribution during both leucine and serine starvation (Figures 5B and S4D, black lines).

To test further the role of translation abortion at ribosome pause sites in determining the distribution of ribosome occupancy along mRNAs, we analyzed three subsets of *E. coli* genes with varying codon usage patterns (Figure 5C). These gene sets had different intragenic locations of the three leucine codons CUA, CUC, and CUU that result in ribosome pausing during leucine starvation (Figure 1B). These three codons were present at a high frequency within the first 300 nt in the first set (Figure 5C, red, 323 genes), between 300 and 600 nt in the second set (Figure 5C, green, 70 genes), and at a low frequency throughout the third set (Figure 5C, blue, 337 genes). The whole-cell model incorporating abortion predicted a decreased ribosome occupancy following the mRNA region where the CUA, CUC, and CUU codons were present at high frequency in these gene sets (Figure 5D). This prediction matched the measured distribution of ribosome occupancy for all three of the gene sets (Figure 5E). By contrast, a model that incorporated only ribosome traffic jams did not recapitulate the measured distribution of ribosome occupancy in the three gene sets (Figure S4E). Together, these observations indicate that incorporating abortion at ribosome pause sites in our whole-cell model of translation is necessary for quantitative consistency with the measured ribosome occupancy along mRNAs during starvation for single amino acids in *E. coli*.

Translation Abortion and Its Effectors during Amino Acid Starvation

Based on the prediction of translation abortion from our analysis of the measured ribosome occupancy, we looked for abortion events at ribosome pause sites using a *yfp* reporter system. We constructed synonymous variants of *yfp* that encoded a 3xFLAG epitope at the N terminus for detection of incomplete polypeptides and that had a single leucine starvation-sensitive CTA codon at one of three different locations along *3xflag-yfp* (Figure 6A). During leucine starvation, we detected shorter-length polypeptide fragments whose size was consistent with premature abortion at the CUA codon (Figure 6B).

Paused ribosomes with an empty A site are stable in vitro (Ivanova et al., 2005), which suggests a role for a *trans*-acting factor in mediating abortion at ribosome pause sites during leucine starvation. Hence, we tested the role of four known abortion-mediating factors in *E. coli*—tmRNA (Keiler et al., 1996), RF3 (Zaher and Green, 2011), ArfA (Chadani et al., 2010), and ArfB (Chadani et al., 2011)—by deleting the genes for each of these factors individually (Figure 6C). Deletion of the gene encoding *tmRNA*, a chimeric transfer-messenger RNA that releases paused ribosomes and tags the incomplete polypeptide for proteolysis (Keiler et al., 1996), caused a significant increase in the ratio of the incomplete-to-full-length YFP (Figure 6C). Further, complementation with a $tmRNA_{His6}$ mutant (Roche and Sauer, 2001), which adds a modified His6 proteolysis-resistant tag but still causes ribosome release, revealed an incomplete YFP polypeptide with a His6 epitope upon immunoprecipitation (Figure 6D). Together, these experiments suggest that tmRNA mediates abortion at ribosome pause sites during leucine starvation. This conclusion is consistent with a previously ascribed role for tmRNA during amino acid starvation (Garza-Sánchez et al., 2008; Li et al., 2008). However, in contrast to these studies and previous in vitro experiments (Ivanova et al., 2004), we did not find evidence for significant mRNA cleavage near the pause site during amino acid starvation (Figure S5A). Furthermore, the measured total mRNA density around the pause site did not indicate appreciable degradation of the region 3′ to the pause site (Figure S5B). Finally, ribosome profiling in a *ΔtmRNA* strain showed only a slight decrease in ribosome occupancy at the 5′ end of mRNAs compared to a $tmRNA^{+}$ strain during leucine starvation (Figure S5C). This observation suggests that abortion is still efficient in the absence of tmRNA and is likely mediated by the abortion-mediating factor ArfA. Such an auxillary role for ArfA in the absence of tmRNA is supported by earlier studies, which found that both the *arfA* mRNA and a truncated but functional form of the ArfA protein are highly stabilized by the deletion of *tmRNA* (Garza-Sánchez et al., 2011) and that double knockout of *arfA* and *tmRNA* is synthetic lethal (Chadani et al., 2010).

We then tested whether ribosome pausing and abortion also affects the expression level of an endogenous *E. coli* protein, the sigma factor RpoS, that is highly upregulated at the

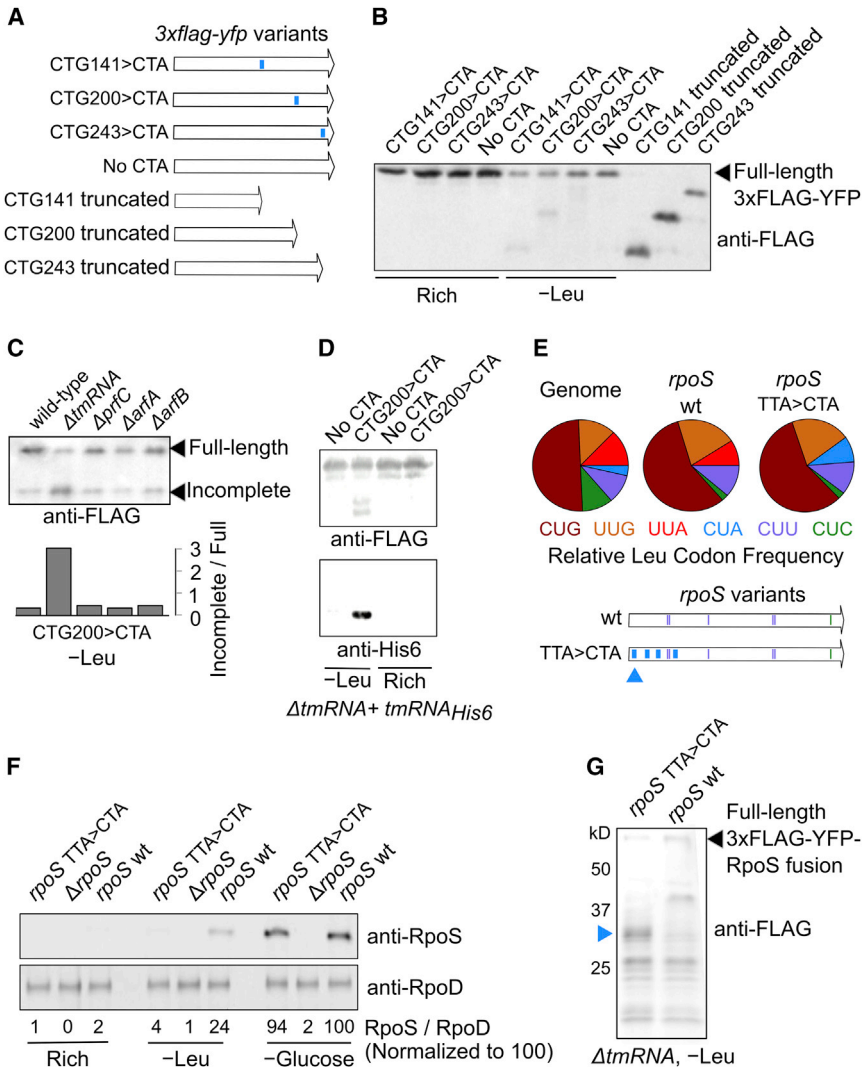

Figure 6. Translation Abortion and Its Effectors during Amino Acid Starvation

(A) Schematic of *3xflag-yfp* reporter variants with either single CTG > CTA substitutions (indicated in blue) or truncated at one of three locations.

(B) Western blot using anti-FLAG antibody for the *3xflag-yfp* variants shown in (A).

(C) Western blot with anti-FLAG antibody of the CTG200 > CTA variant of *yfp* during leucine starvation in strains with deletion of one of four different genes encoding factors that mediate translation abortion (*tmRNA*, *prfC*, *arfA*, *arfB*). "Wild-type" refers to the parent leucine auxotroph strain. The bottom panel indicates the densitometric ratio of these two bands.

(D) (Top) Immunoprecipitation with anti-FLAG antibody of CTG200 > CTA *yfp* variant expressed during leucine starvation in a *ΔtmRNA* strain with a $tmRNA_{His6}$ mutant. (Bottom) $tmRNA_{His6}$ activity detected with an anti-His6 antibody.

(E) (Pie charts) Relative frequency of the six leucine codons across all coding sequences in the genome, in the *rpoS* wild-type coding sequence, and in the *rpoS* synonymous variant. Four TTA codons were replaced by CTA codons in the *rpoS* synonymous variant at the locations indicated by thick blue bars. The thin blue and green bars correspond to the location of the CTC and CTT codons in the *rpoS* WT and synonymous variant. Blue triangle indicates the location of the first ribosome pause site encoded by the CTA codon during leucine starvation.

(F) Western blot against the RpoS protein (top) and RpoD protein (bottom) during nutrient-rich growth, leucine starvation, and glucose starvation. The *rpoS* wild-type coding sequence at the native chromosomal locus was either deleted (*ΔrpoS*) or replaced by the *rpoS* TTA > CTA synonymous variant without additional selection markers. Numbers between the two panels indicate the normalized densitometric ratio of the RpoS and RpoD bands for each lane.

(G) Western blot with anti-FLAG antibody against 3xFLAG-YFP-RpoS fusion proteins during leucine starvation. Approximate molecular weight in kilodaltons (kD) was estimated using a protein ladder. Blue triangle corresponds to the approximate location of the expected truncated peptide caused by ribosome abortion at the first pause site in the *rpoS* TTA > CTA synonymous variant (indicated as a blue triangle in E). See also Figure S5 and Table S2.

transcriptional level in response to leucine starvation (Subramaniam et al., 2013a). Ribosome pause sites encoded by the two leucine codons CTA and CTC during leucine starvation are underrepresented in the *rpoS* protein coding sequence in comparison to their average frequency in the genome (Figure 6E), which suggests that ribosome pause sites during leucine starvation are selected against in the *rpoS* coding sequence due to their adverse effect on the expression of this critical stress response protein. To test the effect of ribosome pause sites on RpoS expression, we substituted, at the chromosomal *rpoS* locus, four leucine TTA codons with the synonymous CTA codons that encode ribosome pause sites (Figure 6E, thick blue bars). Western blotting indicated that the expression level of RpoS decreased ~6-fold during leucine starvation due to the presence of the CTA codons in the *rpoS* coding sequence (Figure 6F). This decrease was specific to leucine starvation, as the synonymous substitutions did not significantly affect the expression of RpoS during glucose starvation, which also strongly upregulates RpoS (Figure 6F). By fusing 3xFLAG-YFP to the N terminus of RpoS, we detected a truncated peptide (Figure 6G, blue triangle) whose size is consistent with translation abortion at the first ribosome pause site in the *rpoS* synonymous variant during leucine starvation (Figure 6E, blue triangle).

Effect of Translation Abortion on Protein Expression during Amino Acid Starvation

Previous studies have suggested that the primary function of abortion mediated by factors such as tmRNA is to rescue inactive mRNA-bound ribosomes during stress and thereby increase the translational capacity in the cell (Moore and Sauer, 2007). To quantify this effect of abortion on ribosome rescue and translational capacity, we tracked the number of free ribosomes and

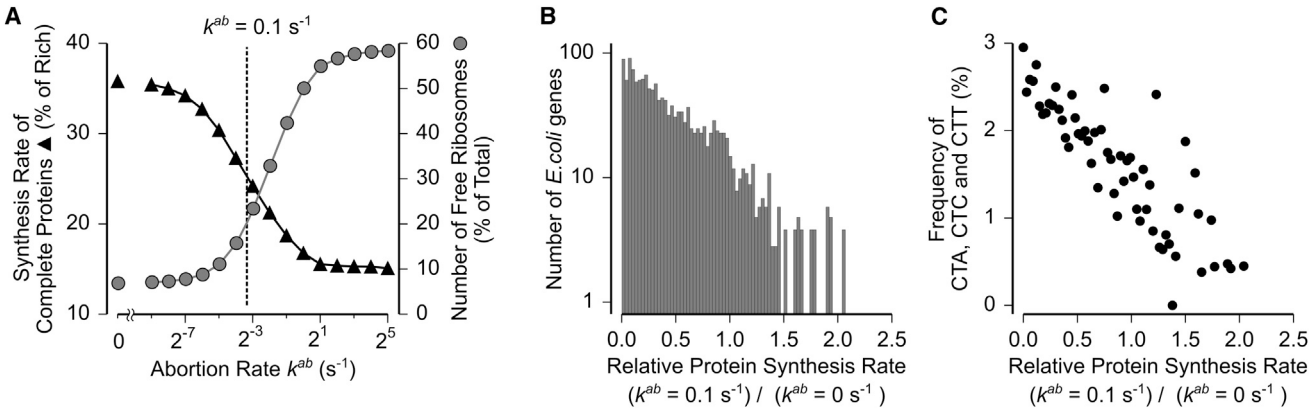

Figure 7. Effect of Translation Abortion on Protein Expression

(A) Effect of varying abortion rate constant (k^{ab}) on the number of free ribosomes in the cell (gray circles) and the global synthesis rate of complete proteins (black triangles) during leucine starvation calculated from whole-cell model. The value k^{ab} = 0.1 s^{-1} that fits the measured ribosome occupancy (black line in Figure 5B) is indicated as a dashed line.

(B) Effect of non-zero abortion rate constant on the synthesis rate of individual *E. coli* proteins during leucine starvation calculated from the whole-cell model.

(C) Average frequency of the three leucine codons CTA, CTC, and CTT for genes in each of the histogram bins in (B). Only genes with greater than ten leucine codons were considered in (B) and (C).

See also Figure S6.

the global synthesis rate of proteins as a function of the abortion rate in our whole-cell model (Figures 7A and S6). Based on earlier work (Bremer and Dennis, 2008), we assumed that 15% of the ribosomes in a cell are free (not bound to mRNAs) during nutrient-rich growth. In the absence of abortion (k^{ab} = 0 s^{-1}), starvation for leucine decreased the fraction of free ribosomes in the cell to 7% (Figure 7A, leftmost circle). Increasing the rate of abortion during leucine starvation gradually rescued the fraction of free ribosomes to a maximum of ~60% in our model (Figure 7A, rightmost circle). We then examined the effect of abortion on global protein expression using our whole-cell model. In the absence of abortion (k^{ab} = 0 s^{-1}), leucine starvation decreased the synthesis rate of complete proteins in the cell to 35% of its value during nutrient-rich growth (Figure 7A, leftmost triangle). Increasing the rate of abortion during leucine starvation further decreased the global synthesis rate to a minimum of ~15% (Figure 7A, rightmost triangle). Notably, increasing the abortion rate had widely different effects on protein expression from individual mRNAs during leucine starvation (Figure 7B). Proteins with higher expression level upon increasing the abortion rate also had a lower frequency of ribosome pause sites in the corresponding mRNAs (Figure 7C). As a result, protein expression from these mRNAs is less susceptible to abortion, and their translation initiation rate is increased by the released ribosomes due to abortion from other mRNAs. Thus, our model predicts that abortion enhances the translation of mRNAs in a selective manner even though it can have a deleterious effect on global protein expression during amino acid starvation.

DISCUSSION

Here, we formulated a biophysical model of translation in *E. coli* by leveraging the near single-codon resolution of the ribosome profiling method. Notably, we constrained our model not only in the initiation-limited regime of nutrient-rich growth, but also in the regime of amino acid starvation, during which the elongation rate of ribosomes has a large effect on the measured ribosome occupancy. By contrast, previous computational models of translation used data solely from initiation-limited regimes, with the consequence that mechanistic features of the elongation stage of translation were not fully constrained (Shah et al., 2013; Tuller et al., 2010). As our results generally illustrate, the exact mechanistic features assumed for the elongation stage have a critical role in models of translation, and changing these features qualitatively alters several of the model predictions.

Consistency between ribosome profiling measurements and our model suggests that the concentration of aminoacyl-tRNAs does not limit the elongation rate of ribosomes at most codons during nutrient-rich growth. This conclusion relies on our assumption that biases in the generation and analysis of ribosome footprinting data are sufficiently small such that the measured ribosome occupancy at codons reflects the residence times of ribosomes with an empty A site at these codons. This assumption is partly supported by our observation that differences in ribosome occupancy at codons during starvation for their cognate amino acid are consistent with their corresponding effect on protein expression. A more direct test of our conclusion will be to characterize the effect of overexpressing low-abundance tRNA isoacceptors on the measured ribosome occupancy during nutrient-rich growth. Our model still predicts a small variation in ribosome occupancy at codons that is correlated with tRNA abundance, the exact magnitude of which depends on the k_{cat}/K_M for ribosome-tRNA association (Figure 3A, vertical axis). Although we predict that this small variation neither limits the ribosome elongation rate at most codons nor affects protein levels during nutrient-rich growth on the physiological timescale of protein synthesis, it can nevertheless leave an evolutionary signature on protein coding sequences and thus underlie the

widely observed correlation between tRNA abundance and codon frequency in microorganisms (Andersson and Kurland, 1990; Drummond and Wilke, 2008; Wallace et al., 2013).

Our analysis of aminoacylation kinetics raises the interesting possibility that cells might utilize differential aminoacylation rates of tRNA isoacceptors as a mechanism to regulate the elongation rate of codons specifically during nutrient stress. Further, small differences in aminoacylation rate between tRNA isoacceptors might also modulate mis-aminocylation rates during other stresses (Netzer et al., 2009) while having little or no deleterious effect on translation during nutrient-rich growth when aminoacylation is not limiting for elongation.

Our work provides in vivo evidence for the widespread occurrence of ribosome traffic jams in response to pausing of a leading ribosome. However, we found that translation abortion at ribosome pause sites is the primary determinant of ribosome occupancy along mRNAs during amino acid starvation. Although abortion from non-stop mRNAs is thought to increase global protein expression during nutrient-rich growth (Moore and Sauer, 2007), our whole-cell modeling suggests that abortion of paused ribosomes during nutrient stress might have the function of enabling selective translation from specific mRNAs. Additionally, releasing nascent polypeptides from paused ribosomes by abortion might facilitate their proteolysis and prevent protein misfolding during stress. However, previous studies have found that eliminating the ability of the abortion-mediating factor tmRNA to target nascent polypeptides to proteolysis does not significantly alter the cellular response to stress (Abo et al., 2002; Huang et al., 2000), suggesting that prevention of protein misfolding is not the primary cellular function of abortion-mediating factors during stress.

The four processes that we modeled in our study (Figure 2) are an essential part of protein synthesis in both bacteria and eukaryotes. Hence, our analysis in *E. coli* can be readily extended to eukaryotes, where ribosome profiling has revealed that a variety of stresses result in a slow elongation rate (Liu et al., 2013; Shalgi et al., 2013). It will also be useful to integrate our whole-cell model of translation with quantitative models of other cellular processes such as transcription (Brewster et al., 2014) and metabolism (Bordbar et al., 2014). Such an integrated model can shed light on the complex interplay between metabolism and gene expression that occurs during environmental changes (Subramaniam et al., 2013b).

EXPERIMENTAL PROCEDURES

Construction of all strains and plasmids (listed in Table S2), western blots, and northern blots were performed using standard molecular biology techniques (Extended Experimental Procedures).

Ribosome Profiling

Ribosome profiling was carried out as described previously (Li et al., 2012; Oh et al., 2011), with the following modifications. To accurately capture the ribosome occupancy on mRNAs with single-codon resolution, we flash froze the cells immediately upon harvesting and stabilized ribosomes with the translation inhibitor chloramphenicol only at the lysis stage. Cells were lysed using glass beads (G1277, Sigma, vortex 10 × 30 s at 4°C with 60 s cooling on ice in between). Micrococcal nuclease digestion was carried out with 1 U Worthington Biochemicals MNase per μg of nucleic acid, as measured by A_{260}. Monosome-protected mRNA footprints between 20 and 40 nt were size selected by polyacrylamide gel electrophoresis for monosome sequencing. For disome sequencing, the disome peak was collected from the MNase-treated polysomes after sucrose-gradient fractionation, and fragments between 50 and 80 nt were used for sequencing. For total mRNA sequencing, the Microbe Express kit (Ambion) was used for subtracting rRNA from total mRNA and then fragmented using a bicarbonate buffer (Ingolia et al., 2009) for 20 min. For library construction, polyA-tailing (Ingolia et al., 2009) was used instead of linker ligation.

High-Throughput Sequencing Data Analysis

Analysis steps were similar to that in previous ribosome profiling studies (Li et al., 2012; Subramaniam et al., 2013b) and were implemented using Python and Bash programming languages. Full programming code for generating the final figures in our paper starting from raw sequencing data is provided both as an interactive IPython notebook (Perez and Granger, 2007) and as a static HTML file (sequencing_data_analysis.html in Data S1). In brief, single-end reads were polyA trimmed and then aligned to the *E. coli* genome (NC_000913.3 build) using Bowtie (Langmead et al., 2009). Aligned reads were trimmed by 8 nt on each side. Each genomic position corresponding to the trimmed read was assigned ribosome occupancy equal to the inverse of the read length. The transcriptome-averaged ribosome occupancy at individual codons for each sample (Figures 1B and 1C) was computed by first averaging the ribosome occupancy at the first nucleotide position of the codon across all occurrences of that codon within each coding sequence and then by averaging across all coding sequences that had a minimum average occupancy of one read/codon. Because the start codon and the three stop codons have a high ribosome density during both nutrient-rich growth and starvation, they were excluded in the plots showing all 61 sense codons (Figures 1 and S1) for clarity. The ribosome occupancy profiles around codons (Figures 5A and 5B) were calculated using the same procedure but for the 120 nt region on each side of the codon rather than just the first nucleotide position of the codon. Ribosome occupancy along mRNAs (Figure 6A) was computed by first normalizing the ribosome occupancy at each position of a coding sequence by the average ribosome occupancy for the full coding sequence, and then by averaging this quantity at each position beginning from the start codon across all coding sequences that had a minimum average occupancy of one read/codon.

Whole-Cell Model of *E. coli* Translation

Our whole-cell model for translation (Figure 2) was implemented using the stochastic Gillespie algorithm (Gillespie, 1977). The source code for implementing the kinetic model in Figure 2 was adapted from Shah et al., (2013), with modifications as shown in Data S1. Full programming code for running the simulation and for the subsequent data analysis to generate the final figures in our paper is provided both as an interactive IPython notebook (Perez and Granger, 2007) and as a static HTML file (simulation.html and simulation_data_analysis.html in Data S1). Standard errors of mean for model predictions in all figures are smaller than data markers. Our whole-cell model tracked the state of 44,000 ribosomes, 408,000 tRNA molecules (38 distinct tRNA species), and ~7,500 mRNA molecules (1,518 distinct mRNA species) in the *E. coli* cell (Table S1). The transition rates between different states of each of these molecules are determined by the four rate equations in Figure 2B. The key parameters that control the predictions from our model are the rate constants k for the four processes in Figure 2B. Based on the analysis presented in the main text, we chose a default set of parameters for all of our simulations. Table S1 lists these choices, together with the corresponding references and a footnote explaining the choice (see also Extended Experimental Procedures). We chose parameters corresponding to a cell doubling time of 30 min that we measured during nutrient-rich growth in our experiments.

ACCESSION NUMBERS

Sequencing data are publicly available from Gene Expression Omnibus, accession number GSE51052. Simulation results and programming code for simulation, sequencing data analysis, simulation data analysis and reproduction of figures are publicly available at http://datadryad.org/, http://dx.doi.org/10.5061/dryad.ch352.

SUPPLEMENTAL INFORMATION

Supplemental Information includes Extended Experimental Procedures, six figures, two tables, and one data file and can be found with this article online at http://dx.doi.org/10.1016/j.cell.2014.10.043.

AUTHOR CONTRIBUTIONS

A.R.S. and E.K.O. designed research. A.R.S. performed research and analyzed data with input from B.M.Z. A.R.S. and E.K.O. wrote the manuscript.

ACKNOWLEDGMENTS

We thank J. Calarco, P. Cluzel, V. Denic, A. Murray, and C. Shoemaker for discussions; G.W. Li and E. Oh for advice on ribosome profiling; G.L. Chew and A. Gutu for advice on northern blotting; H. Aiba for the XL001 strain; P. Shah for clarifications on the yeast model; and K. Amarnath, A. Buskirk, S. Chandrasekaran, A. Darnell, G.W. Li, W. Moebius, J. Moffitt, P. Shah, and E. Wallace for comments on the manuscript. The computations in this paper were run on the Odyssey cluster supported by the FAS Division of Science, Research Computing Group at Harvard University. This research was supported by an NIH K99 Pathway to Independence Award GM107113 (A.R.S.) and by the Howard Hughes Medical Institute (E.K.O.).

Received: June 16, 2014
Revised: August 18, 2014
Accepted: October 21, 2014
Published: November 20, 2014

REFERENCES

Abo, T., Ueda, K., Sunohara, T., Ogawa, K., and Aiba, H. (2002). SsrA-mediated protein tagging in the presence of miscoding drugs and its physiological role in Escherichia coli. Genes Cells *7*, 629–638.

Andersson, S.G., and Kurland, C.G. (1990). Codon preferences in free-living microorganisms. Microbiol. Rev. *54*, 198–210.

Bilgin, N., and Ehrenberg, M. (1994). Mutations in 23 S ribosomal RNA perturb transfer RNA selection and can lead to streptomycin dependence. J. Mol. Biol. *235*, 813–824.

Bordbar, A., Monk, J.M., King, Z.A., and Palsson, B.O. (2014). Constraint-based models predict metabolic and associated cellular functions. Nat. Rev. Genet. *15*, 107–120.

Bremer, H., and Dennis, P. (2008). Modulation of chemical composition and other parameters of the cell at different exponential growth rates. In EcoSal-*Escherichia coli* and *Salmonella*: Cellular and Molecular Biology, A. Bock, R. Curtiss, III, J.B. Kaper, P.D. Karp, F.C. Neidhardt, T. Nystrom, J.M. Slauch, C.L. Squires, D. Ussery, and E. Schaechter, eds. (Washington, DC: ASM Press).

Brewster, R.C., Weinert, F.M., Garcia, H.G., Song, D., Rydenfelt, M., and Phillips, R. (2014). The transcription factor titration effect dictates level of gene expression. Cell *156*, 1312–1323.

Chadani, Y., Ono, K., Ozawa, S., Takahashi, Y., Takai, K., Nanamiya, H., Tozawa, Y., Kutsukake, K., and Abo, T. (2010). Ribosome rescue by Escherichia coli ArfA (YhdL) in the absence of trans-translation system. Mol. Microbiol. *78*, 796–808.

Chadani, Y., Ono, K., Kutsukake, K., and Abo, T. (2011). Escherichia coli YaeJ protein mediates a novel ribosome-rescue pathway distinct from SsrA- and ArfA-mediated pathways. Mol. Microbiol. *80*, 772–785.

Dittmar, K.A., Sørensen, M.A., Elf, J., Ehrenberg, M., and Pan, T. (2005). Selective charging of tRNA isoacceptors induced by amino-acid starvation. EMBO Rep. *6*, 151–157.

Dong, H., Nilsson, L., and Kurland, C.G. (1996). Co-variation of tRNA abundance and codon usage in Escherichia coli at different growth rates. J. Mol. Biol. *260*, 649–663.

Drummond, D.A., and Wilke, C.O. (2008). Mistranslation-induced protein misfolding as a dominant constraint on coding-sequence evolution. Cell *134*, 341–352.

Elf, J., Nilsson, D., Tenson, T., and Ehrenberg, M. (2003). Selective charging of tRNA isoacceptors explains patterns of codon usage. Science *300*, 1718–1722.

Fender, A., Sissler, M., Florentz, C., and Giegé, R. (2004). Functional idiosyncrasies of tRNA isoacceptors in cognate and noncognate aminoacylation systems. Biochimie *86*, 21–29.

Garza-Sánchez, F., Gin, J.G., and Hayes, C.S. (2008). Amino acid starvation and colicin D treatment induce A-site mRNA cleavage in Escherichia coli. J. Mol. Biol. *378*, 505–519.

Garza-Sánchez, F., Schaub, R.E., Janssen, B.D., and Hayes, C.S. (2011). tmRNA regulates synthesis of the ArfA ribosome rescue factor. Mol. Microbiol. *80*, 1204–1219.

Gillespie, D.T. (1977). Exact stochastic simulation of coupled chemical reactions. J. Phys. Chem. *81*, 2340–2361.

Gustafsson, C., Govindarajan, S., and Minshull, J. (2004). Codon bias and heterologous protein expression. Trends Biotechnol. *22*, 346–353.

Guydosh, N.R., and Green, R. (2014). Dom34 rescues ribosomes in 3′ untranslated regions. Cell *156*, 950–962.

Harris, C.L., and Marashi, F. (1980). Two kinetically distinct tRNAile isoacceptors in Escherichia coli C6. Nucleic Acids Res. *8*, 2023–2037.

Huang, C., Wolfgang, M.C., Withey, J., Koomey, M., and Friedman, D.I. (2000). Charged tmRNA but not tmRNA-mediated proteolysis is essential for Neisseria gonorrhoeae viability. EMBO J. *19*, 1098–1107.

Ingolia, N.T., Ghaemmaghami, S., Newman, J.R.S., and Weissman, J.S. (2009). Genome-wide analysis in vivo of translation with nucleotide resolution using ribosome profiling. Science *324*, 218–223.

Ivanova, N., Pavlov, M.Y., Felden, B., and Ehrenberg, M. (2004). Ribosome rescue by tmRNA requires truncated mRNAs. J. Mol. Biol. *338*, 33–41.

Ivanova, N., Pavlov, M.Y., and Ehrenberg, M. (2005). tmRNA-induced release of messenger RNA from stalled ribosomes. J. Mol. Biol. *350*, 897–905.

Jacques, N., and Dreyfus, M. (1990). Translation initiation in Escherichia coli: old and new questions. Mol. Microbiol. *4*, 1063–1067.

Keiler, K.C., and Feaga, H.A. (2014). Resolving nonstop translation complexes is a matter of life or death. J. Bacteriol., JB.01490–14.

Keiler, K.C., Waller, P.R.H., and Sauer, R.T. (1996). Role of a peptide tagging system in degradation of proteins synthesized from damaged messenger RNA. Science *271*, 990–993.

Kudla, G., Murray, A.W., Tollervey, D., and Plotkin, J.B. (2009). Coding-sequence determinants of gene expression in Escherichia coli. Science *324*, 255–258.

Langmead, B., Trapnell, C., Pop, M., and Salzberg, S.L. (2009). Ultrafast and memory-efficient alignment of short DNA sequences to the human genome. Genome Biol. *10*, R25.

Li, X., Yagi, M., Morita, T., and Aiba, H. (2008). Cleavage of mRNAs and role of tmRNA system under amino acid starvation in Escherichia coli. Mol. Microbiol. *68*, 462–473.

Li, G.-W., Oh, E., and Weissman, J.S. (2012). The anti-Shine-Dalgarno sequence drives translational pausing and codon choice in bacteria. Nature *484*, 538–541.

Li, G.-W., Burkhardt, D., Gross, C., and Weissman, J.S. (2014). Quantifying absolute protein synthesis rates reveals principles underlying allocation of cellular resources. Cell *157*, 624–635.

Liu, B., Han, Y., and Qian, S.-B. (2013). Cotranslational response to proteotoxic stress by elongation pausing of ribosomes. Mol. Cell *49*, 453–463.

Moore, S.D., and Sauer, R.T. (2005). Ribosome rescue: tmRNA tagging activity and capacity in Escherichia coli. Mol. Microbiol. *58*, 456–466.

Moore, S.D., and Sauer, R.T. (2007). The tmRNA system for translational surveillance and ribosome rescue. Annu. Rev. Biochem. *76*, 101–124.

Myers, G., Blank, H.U., and Söll, D. (1971). A comparative study of the interactions of Escherichia coli leucyl-, seryl-, and valyl-transfer ribonucleic acid synthetases with their cognate transfer ribonucleic acids. J. Biol. Chem. *246*, 4955–4964.

Netzer, N., Goodenbour, J.M., David, A., Dittmar, K.A., Jones, R.B., Schneider, J.R., Boone, D., Eves, E.M., Rosner, M.R., Gibbs, J.S., et al. (2009). Innate immune and chemically triggered oxidative stress modifies translational fidelity. Nature *462*, 522–526.

Oh, E., Becker, A.H., Sandikci, A., Huber, D., Chaba, R., Gloge, F., Nichols, R.J., Typas, A., Gross, C.A., Kramer, G., et al. (2011). Selective ribosome profiling reveals the cotranslational chaperone action of trigger factor in vivo. Cell *147*, 1295–1308.

Pavlov, M.Y., and Ehrenberg, M. (1996). Rate of translation of natural mRNAs in an optimized in vitro system. Arch. Biochem. Biophys. *328*, 9–16.

Perez, F., and Granger, B.E. (2007). IPython: A System for Interactive Scientific Computing. Comput. Sci. Eng. *9*, 21–29.

Qian, W., Yang, J.-R., Pearson, N.M., Maclean, C., and Zhang, J. (2012). Balanced codon usage optimizes eukaryotic translational efficiency. PLoS Genet. *8*, e1002603.

Roche, E.D., and Sauer, R.T. (2001). Identification of endogenous SsrA-tagged proteins reveals tagging at positions corresponding to stop codons. J. Biol. Chem. *276*, 28509–28515.

Shah, P., Ding, Y., Niemczyk, M., Kudla, G., and Plotkin, J.B. (2013). Rate-limiting steps in yeast protein translation. Cell *153*, 1589–1601.

Shalgi, R., Hurt, J.A., Krykbaeva, I., Taipale, M., Lindquist, S., and Burge, C.B. (2013). Widespread regulation of translation by elongation pausing in heat shock. Mol. Cell *49*, 439–452.

Shoemaker, C.J., and Green, R. (2012). Translation drives mRNA quality control. Nat. Struct. Mol. Biol. *19*, 594–601.

Sørensen, M.A. (2001). Charging levels of four tRNA species in Escherichia coli Rel(+) and Rel(-) strains during amino acid starvation: a simple model for the effect of ppGpp on translational accuracy. J. Mol. Biol. *307*, 785–798.

Sørensen, M.A., Elf, J., Bouakaz, E., Tenson, T., Sanyal, S., Björk, G.R., and Ehrenberg, M. (2005). Over expression of a tRNA(Leu) isoacceptor changes charging pattern of leucine tRNAs and reveals new codon reading. J. Mol. Biol. *354*, 16–24.

Subramaniam, A.R., Pan, T., and Cluzel, P. (2013a). Environmental perturbations lift the degeneracy of the genetic code to regulate protein levels in bacteria. Proc. Natl. Acad. Sci. USA *110*, 2419–2424.

Subramaniam, A.R., DeLoughery, A., Bradshaw, N., Chen, Y., O'Shea, E., Losick, R., and Chai, Y. (2013b). A serine sensor for multicellularity in a bacterium. eLife *2*, e01501.

Tuller, T., Carmi, A., Vestsigian, K., Navon, S., Dorfan, Y., Zaborske, J., Pan, T., Dahan, O., Furman, I., and Pilpel, Y. (2010). An evolutionarily conserved mechanism for controlling the efficiency of protein translation. Cell *141*, 344–354.

Varenne, S., Buc, J., Lloubes, R., and Lazdunski, C. (1984). Translation is a non-uniform process. Effect of tRNA availability on the rate of elongation of nascent polypeptide chains. J. Mol. Biol. *180*, 549–576.

Vind, J., Sørensen, M.A., Rasmussen, M.D., and Pedersen, S. (1993). Synthesis of proteins in Escherichia coli is limited by the concentration of free ribosomes. Expression from reporter genes does not always reflect functional mRNA levels. J. Mol. Biol. *231*, 678–688.

Wallace, E.W.J., Airoldi, E.M., and Drummond, D.A. (2013). Estimating selection on synonymous codon usage from noisy experimental data. Mol. Biol. Evol. *30*, 1438–1453.

Welch, M., Govindarajan, S., Ness, J.E., Villalobos, A., Gurney, A., Minshull, J., and Gustafsson, C. (2009). Design parameters to control synthetic gene expression in Escherichia coli. PLoS ONE *4*, e7002.

Wintermeyer, W., Peske, F., Beringer, M., Gromadski, K.B., Savelsbergh, A., and Rodnina, M.V. (2004). Mechanisms of elongation on the ribosome: dynamics of a macromolecular machine. Biochem. Soc. Trans. *32*, 733–737.

Wolin, S.L., and Walter, P. (1988). Ribosome pausing and stacking during translation of a eukaryotic mRNA. EMBO J. *7*, 3559–3569.

Yegian, C.D., Stent, G.S., and Martin, E.M. (1966). Intracellular condition of Escherichia coli transfer RNA. Proc. Natl. Acad. Sci. USA *55*, 839–846.

Zaher, H.S., and Green, R. (2011). A primary role for release factor 3 in quality control during translation elongation in Escherichia coli. Cell *147*, 396–408.

Zhang, S., Goldman, E., and Zubay, G. (1994). Clustering of low usage codons and ribosome movement. J. Theor. Biol. *170*, 339–354.

EXTENDED EXPERIMENTAL PROCEDURES

Bacterial Strains

E. coli strain MG1655-*leuB*::*kan* was used for leucine starvation and *E. coli* strain BW25113-*serA*::kan was used for serine starvation. Amino acid auxotrophic strains were obtained from the BW25113 Keio-knockout collection (Baba et al., 2006) of the Coli Genetic Stock Center, Yale. *leuB*::*kan* marker was transferred to the MG1655 background by λ-Red mediated recombination (Datsenko and Wanner, 2000). The same method was also used to transfer *tmRNA*::*cat* from XL001 (gift from H. Aiba) to the MG1655 background. The genes *prfC*, *arfA* and *arfB* were deleted by replacing their full coding sequence with a *kan* marker using the λ-Red method. Before the deletion of these genes, the *kan* marker at the leuB locus was replaced by FRT scars as described (Datsenko and Wanner, 2000). For inducible control of *yfp* in western blotting experiments, a *tet* repressor gene was inserted into the λ *attB* site by site-specific recombination as described previously (Lutz and Bujard, 1997). The *rpoS* TTA > CTA synonymous variant was custom synthesized (IDT) and inserted into the chromosome using a two-step λ-Red recombination method. First, the *rpoS* wild-type coding sequence at its native chromosomal locus was replaced by a *kan-ccdB* marker from pKD45 (gift of H. Berg). Next, the *kan-ccdB* marker was replaced without any residual scars by the *rpoS* TTA > CTA synonymous variant using counter-selection against the *ccdB* marker.

Plasmids

All *yfp* and *3xflag-yfp* reporters were expressed from a low-copy SC101* *ori* plasmid (3-4 copies per cell) that were derivatives of pAS04-*yfp0* (Subramaniam et al., 2013a). All synonymous mutations were introduced into the *yfp* gene using a commercial site-directed mutagenesis kit (Stratagene). The 22 amino acid 3xFLAG epitope at the N terminus of YFP in the western blotting experiments was encoded by the DNA sequence: 'GACTACAAAGACCATGACGGTGATTATAAAGATCATGACATCGACTACAAG GATGACGATGACAAG'. The *3xflag-yfp-rpos* fusion was constructed by inserting a GGSGGS linker encoding sequence and the *rpoS* coding sequence (either wild-type or the TTA > CTA variant) before the stop codon of 3xflag-yfp in the pAS04-*yfp0* vector backbone. The $tmRNA_{His6}$ mutant was constructed by amplifying the wild-type *tmRNA-smpB* gene cluster (2752806nt to 2754180nt in the *E. coli* genome sequence file NC_000913.fna) from the *E. coli* genome using PCR. The wild-type sequence was modified to the previously described His6 mutant sequence (Roche and Sauer, 2001) using fusion PCR, and ligated between the AatII and XhoI restriction sites of pAS04 carrying the *3xflag-yfp* reporter gene for low-copy expression from the same vector.

Bacterial Growth

For general purposes, *E. coli* was grown in Luria-Bertani broth at 37°C. For all experiments, overnight cultures were grown at 30°C, 200 rpm in a MOPS-based, rich, defined medium (Neidhardt et al., 1974) modified to contain either 1 mM leucine or 10 mM serine for the respective amino acid auxotrophs. Overnight cultures were diluted 1:100 into fresh medium. After growth for 3 hr at 30°C with shaking at 200 rpm to an OD_{600} ~0.6, cultures were starved for the respective auxotrophic amino acids for 30 min in the MOPS-based rich medium without the single auxotrophic amino acid, and harvested for ribosome profiling, Northern blotting or western blotting. Northern blotting for ribosome footprinting (Figure 4D) was carried out in strains with constitutive YFP expression. For all western blotting experiments and the Northern blotting experiment against the total mRNA (Figure S5A), YFP or YFP-RpoS fusion synthesis was induced only during starvation (and as a control, for an equal time in amino acid rich medium) using 200 ng/ml of anhydrotetracycline.

Western Blotting

1 ml cultures were spun down and then lysed in CellLytic B reagent (Sigma). Western blotting protocol as described (Subramaniam et al., 2013a) was carried out with M2 Anti-FLAG antibody (Sigma) for detecting 3xFLAG epitopes and an anti-His6 antibody (Cell Signaling) for detecting $tmRNA_{His6}$ tagging activity. RpoS and RpoD proteins were detected using corresponding monoclonal antibodies (Abcam 81737 and Neoclone WP004).

Northern Blotting

For northen blotting against ribosome footprints, cell harvesting, lysis, nuclease-digestion and sucrose-gradient fractionation was done as described in the ribosome profiling protocol. During fractionation, in addition to monosomes, 6 ml of the gradient corresponding to higher polysome fractions was collected and pooled together. Purified RNA was then separated on 15% TBE-Urea gels using parameters identical to that in the ribosome profiling protocol.

For northern blotting against total RNA, total RNA was extracted from 1ml of cultures using the RNAsnap method (Stead et al., 2012), and separated on a 5% TBE-Urea gel (Bio-Rad) at 200V for 120 min.

RNA (either total or ribosome footprints) was transferred to a positively-charged Nylon membrane and UV-crosslinked (Stratagene 2400 lamp). A P^{32}-labeled 300 nt antisense RNA probe complementary to −250nt to +50nt of the CTG200 > CTA substitution in *yfp* was synthesized by in vitro transcription (Maxiscript, Ambion). After UV crosslinking, the membrane was hybridized overnight together with the probe (PerfectHyb Plus buffer, Sigma) at 68°C with rotation. After washing in high stringency buffer (0.1X SSC, 0.1%SDS), the membrane was imaged for 30 min on a phosphor screen followed by scanning on a Typhoon imager (GE).

Whole-Cell Model of *E. coli* Translation

Our whole-cell model for translation (Figure 2) was implemented using the stochastic Gillespie algorithm (Gillespie, 1977). We have summarized below our choices for the three key aspects of our model: (1) the molecular species and their state space, (2) the transition rates between the molecular states, (3) the model parameters. The source code for implementing the kinetic model in Figure 2 was adapted from (Shah et al., 2013) with modifications as described below and in Data S1. Full programming code for running the simulation and for the subsequent data analysis to generate the final figures in our paper is provided both as an interactive IPython notebook (Perez and Granger, 2007) and as a static HTML file (simulation.html and simulation_data_analysis.html in Data S1). Standard errors of mean for model predictions in all figures are smaller than data markers.

Molecular Species and Their State Space

Our whole-cell model tracked the state of 44,000 ribosomes, 408,000 tRNA molecules (38 distinct tRNA species) and ~7500 mRNA molecules (1518 distinct mRNA species) in the *E. coli* cell (Table S1). The ribosomes were present in one of two states: free or mRNA-bound. In addition, the identity of the P-site tRNA on each ribosome was tracked when it was mRNA-bound. The tRNAs were present in one of three different states: free aminoacyl-tRNA, free deacylated tRNA and ribosome P-site bound tRNA. Every codon on each of the mRNA molecules was present in one of two states: empty or occupied by the A-site of a translating ribosome.

Transition Rates between Molecular States

Ribosomes transition from a free to an mRNA-bound state by initiation on mRNAs at a rate given by Equation (1) in Figure 2B. Ribosomes transition from mRNA-bound to free either by instantaneous termination once they reach the stop codon of an mRNA or by abortion at ribosome pause sites at a rate given by Equation (4) in Figure 2B. Deacylated tRNAs transition to aminoacyl-tRNAs through aminoacylation by the aminoacyl tRNA synthetases at a rate given by Equation (3) in Figure 2B. The concentration of amino acids is implicitly accounted for through the rate constant k^{aa}. Aminoacyl-tRNAs transition to ribosome-bound P-site tRNAs at the elongation rate given by Equation (2) in Figure 2B. Ribosome-bound P-site tRNAs transition to deacylated tRNAs by elongation, by abortion, or by instantaneous termination at stop codons. Codons on mRNAs transition from an empty to a ribosome-bound state upon arrival of a ribosome by elongation. Codons transition from a ribosome-bound to empty state by either elongation or by abortion of a bound ribosome.

Model Parameters

Based on the analysis presented in the main text, we chose a default set of parameters for all our simulations. Table S1 lists these choices, together with the corresponding references and a footnote explaining the choice. We chose parameters corresponding to a cell doubling time of 30 min that we measured during nutrient-rich growth in our experiments. The key parameters that control the predictions from our model are the rate constants for the four processes in Figure 2B, and the choices for these rate constants are explained in detail below.

To infer the copy number of each mRNA (each ORF was considered a separate mRNA), the total RNA-Seq counts for each mRNA was normalized by the total amount of mRNA in the cell, 4×10^6 nt/cell (Bremer and Dennis, 2008). The mRNA copy number was taken as 1/cell if it was below 1/cell in our calculation. To infer the initiation rate constant k^{in} of each mRNA, first the ribosome profiling counts for each mRNA was normalized by the total number of ribosomes in the cell, 44000 (Bremer and Dennis, 2008), and by the inferred mRNA copy number. This result was multiplied by the average elongation rate, 22 codons per second (Bremer and Dennis, 2008), during nutrient-rich growth. The 1518 mRNA species that had an average ribosome profiling sequencing density of 1 read/codon were considered for the simulation. Initiation rates for mRNAs that did not have at least 10 sequencing reads in both the ribosome profiling and RNA-Seq measurements were assigned the median initiation rate of the remaining mRNAs that passed this threshold.

To calculate the elongation rate of ribosomes at codons, the rate constant for elongation, k^{el}, was taken as 2×10^7 $M^{-1}s^{-1}$ (Bilgin and Ehrenberg, 1994; Pavlov and Ehrenberg, 1996). The concentrations of individual tRNA species and codon-tRNA assignments were from (Dong et al., 1996). The concentrations of individual tRNA species were normalized such that the total tRNA concentration in the cell was 408,000 molecules at a doubling time of 30 min (Bremer and Dennis, 2008). The wobble parameters for codon-tRNA interaction w, were based on (Shah et al., 2013).

The aminoacylation rate constant k^{aa} during nutrient-rich growth, 2×10^{10} $M^{-1}s^{-1}$ was chosen such that all tRNAs were at least 80% aminoacylated. The aminoacylation rate constant during starvation was systematically varied (Figures 3C, 3D). Since the exact value of this parameter is not critical to any of our conclusions, we used a 100-fold reduction in k^{aa} upon starvation as a default choice (Table S1). The difference in aminoacylation rate constants for leucine and serine tRNA isoacceptors was systematically increased until the predicted hierarchy in codon ribosome occupancy (Figures 3D, S2E) matched the experimentally measured hierarchy (Figures 1B, 1C). For clarification, we have illustrated this procedure graphically for the case of leucine starvation (Figure S2D) where, for the equal aminoacylation case, the CUG codon has higher predicted relative ribosome occupancy than the measured value in Figure 1B. When the parameter Δ (definition in Figure S2D) is set to zero, all Leu tRNAs have equal aminoacylation rate constants (left dashed line, Figure S2D). As Δ is increased from 0 to 1, the difference in aminoacylation rate constants between the Leu tRNAs increases continuously. We chose the value of $\Delta = 0.5$ (right dashed line, Figure S2D) which recapitulates the measured hierarchy of ribosome occupancy with reasonable accuracy (Figure 1B). The choice of increasing / decreasing / constant aminoacylation rate constants for each Leu tRNA upon varying Δ was based on whether the tRNA was cognate only to CUG (Leu1), or only to other codons (Leu2, Leu4, Leu5), or to both CUG and other codons (Leu3), respectively.

The abortion rate constant k^{ab} was systematically varied in our work (Figures 5B, 7A). The default value k^{ab} = 0.1 s^{-1} was chosen such that the measured ribosome occupancy profile (Figure 5A) and the predicted ribosome occupancy profile (Figure 5B) were similar. We chose the threshold elongation rate for abortion $R^{el}{}_{threshold}$ to be non-zero and lower than the elongation rate of all codons during nutrient-rich growth.

Our model, despite its whole-cell level, includes only a minimal set of kinetic processes that could be constrained by our ribosome occupancy measurements. For example, we did not explicitly model the diffusion of ribosomes and tRNAs in the cell, nor we did we consider competition among near-cognate tRNA isoacceptors for incorporation at the ribosome A-site (Fluitt et al., 2007; Shah et al., 2013). In our model, these processes are implicitly accounted through the kinetic rate constants for initiation (k_{in}) and elongation (k_{el}), respectively. We also did not consider molecular events that could be potentially important in our study but for which there is no experimental evidence. Notably, we did not consider abortion of jammed ribosomes [Equation (4) in Figure 2B] since abortive mechanisms in bacteria such as tmRNA-mediated ribosome rescue often require an empty A-site (Garza-Sánchez et al., 2006).

In our study, parameters that have been accurately estimated from previous experiments such as the in vivo concentrations of ribosomes, tRNAs and mRNAs (Bremer and Dennis, 2008) were taken as fixed parameters. On the other hand, less certain parameters such as the k_{cat}/K_M for ribosome-tRNA association (k_{el}), the aminoacylation rate constant (k_{aa}) and the abortion rate constant (k_{in}), were systematically varied to test their consistency with ribosome occupancy measurements. Since our estimates for these parameters (Table S1) are not direct in vivo measurements, they should be interpreted as order-of-magnitude approximations and not as exact values.

Our model also reveals that hierarchy of ribosome occupancy at codons during starvation is much more sensitive to the 3-fold variation in the aminoacylation rate constant (k^{aa}) than to the 3-fold variation in elongation rate constant (k^{el}) (Figure 3D versus Figure S2C). This can be understood from the fact that tRNA isoacceptors compete with one another during aminoacylation, which causes their relative aminoacylation rates (and hence the ribosome occupancy at the corresponding codons) to be ultra-sensitive to changes in their aminoacylation rate constants k^{aa} during starvation (Elf, 2004). By contrast, the relative usage of different aa-tRNA isoacceptors during elongation is stoichiometrically constrained by the frequency of the corresponding codons in the transcriptome. Hence, changes in the elongation rate constant k^{el} have only a minor effect on the hierarchy of ribosome occupancy at codons during starvation.

Simulation and Analysis Steps

Full programming code for running the simulation and for the subsequent data analysis to generate the final figures in our paper is provided both as an interactive IPython notebook (Perez and Granger, 2007) and as a static HTML file (simulation.html and simulation_data_analysis.html in Data S1). Transgene overexpression was simulated by expressing 10 randomly chosen variants of three different transgenes (YFP, human insulin, Φ29 DNA polymerase) with a range of Codon Adaptation Index values. During transgene overexpression, the overall number of mRNAs in the cell was kept approximately equal to the wild-type case. The average ribosome occupancy along mRNAs and at codons in the simulation was calculated using a procedure analogous to our ribosome profiling analysis. Specifically, we normalized the ribosome occupancy by its average value along each mRNA and the mRNA copy number. Only mRNAs that had a minimum of 5 initiation events over 500 s of simulation after an initial 1000 s to reach steady state were considered for our analysis. The protein synthesis rate was calculated by multiplying the number of complete proteins synthesized by the length of each protein over 500 s of simulation after an initial 1000 s to reach steady state. Aborted polypeptides were not considered for calculating protein synthesis rate since they are rapidly degraded by the action of the transfer-messenger RNA. Simulation and analysis code for the yeast computational model of translation is provided in yeast_simulation_and_analysis.html.

SUPPLEMENTAL REFERENCES

Baba, T., Ara, T., Hasegawa, M., Takai, Y., Okumura, Y., Baba, M., Datsenko, K.A., Tomita, M., Wanner, B.L., and Mori, H. (2006). Construction of Escherichia coli K-12 in-frame, single-gene knockout mutants: the Keio collection. Mol. Syst. Biol. *2*, 0008.

Bremer, H., Dennis, P., and Ehrenberg, M. (2003). Free RNA polymerase and modeling global transcription in Escherichia coli. Biochimie *85*, 597–609.

Datsenko, K.A., and Wanner, B.L. (2000). One-step inactivation of chromosomal genes in Escherichia coli K-12 using PCR products. Proc. Natl. Acad. Sci. USA *97*, 6640–6645.

Elf, J. (2004). Intracellular flows and fluctuations. PhD thesis (Uppsala, Sweden: Uppsala University).

Fluitt, A., Pienaar, E., and Viljoen, H. (2007). Ribosome kinetics and aa-tRNA competition determine rate and fidelity of peptide synthesis. Comput. Biol. Chem. *31*, 335–346.

Garza-Sánchez, F., Janssen, B.D., and Hayes, C.S. (2006). Prolyl-tRNA(Pro) in the A-site of SecM-arrested ribosomes inhibits the recruitment of transfer-messenger RNA. J. Biol. Chem. *281*, 34258–34268.

Lutz, R., and Bujard, H. (1997). Independent and tight regulation of transcriptional units in Escherichia coli via the LacR/O, the TetR/O and AraC/I1-I2 regulatory elements. Nucleic Acids Res. *25*, 1203–1210.

Neidhardt, F.C., Bloch, P.L., and Smith, D.F. (1974). Culture medium for enterobacteria. J. Bacteriol. *119*, 736–747.

Stead, M.B., Agrawal, A., Bowden, K.E., Nasir, R., Mohanty, B.K., Meagher, R.B., and Kushner, S.R. (2012). RNAsnap™: a rapid, quantitative and inexpensive, method for isolating total RNA from bacteria. Nucleic Acids Res. *40*, e156.

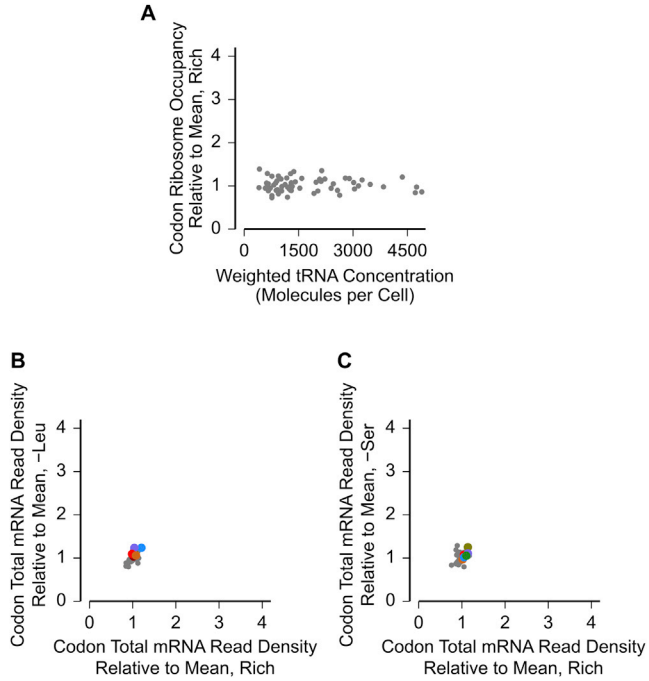

Figure S1. Correlation of tRNA Abundance with Ribosome Occupancy and Total mRNA Density at Codons, Related to Figure 1

(A) Measured ribosome occupancy at the 61 sense codons averaged across the transcriptome as a function of tRNA abundance (Dong et al., 1996). The concentration of isoacceptors for each codon were summed with weights *w* (Figure 2B) to account for differences in codon-anticodon interaction (Supplemental Data).

(B and C) Measured total mRNA read density at the 61 sense codons averaged across the transcriptome. Leucine codons are highlighted in (B) and serine codons are highlighted in (C). Start and stop codons are not shown. The standard error for each codon is smaller than the corresponding data marker.

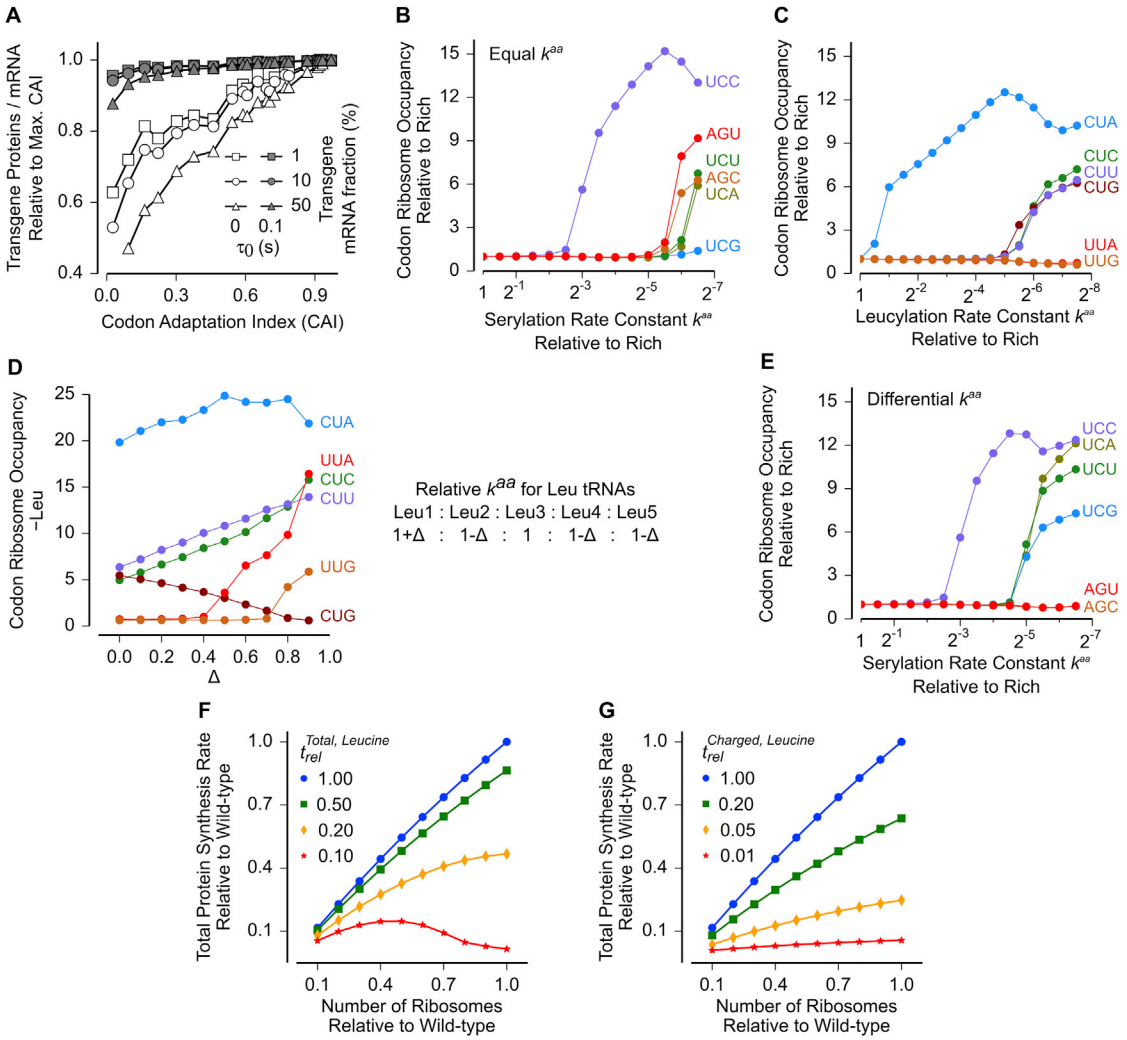

Figure S2. Effect of Elongation and Aminoacylation Kinetics in *S. cervisiae* and in *E. coli*, Related to Figure 3

(A) Amount of transgene proteins produced per mRNA upon overexpression during nutrient-rich growth in *S. cerevisiae* calculated using the model in (Shah et al., 2013). Simulations were run with the time for intra-ribosomal events at a single codon, τ_0 set to either 0 s or 0.1 s. The k_{cat} / K_M for ribosome-ternary complex association, k_{ia}^{el}, was chosen such that the mean elongation rate of ribosomes is approximately equal to the experimentally measured value of 10 s^{-1} in both cases (k_{ia}^{el} = 3.6 × 10^6 $M^{-1}s^{-1}$ for τ_0 = 0 s, k_{ia}^{el} = 3.6 × 10^7 $M^{-1}s^{-1}$ for τ_0 = 0.1 s). All other parameters were identical to that of (Shah et al., 2013).

(C) Mean ribosome occupancy as a function of leucylation rate constant $k^{aa,\,Leu}$ for the six leucine codons calculated from whole-cell model. The elongation rate constants k^{el} for the four leucine codons CUA, CUC, CUU and CUG were based on the measurements of (Sørensen et al., 2005).

(D) Effect of differential aminoacylation rate constants between leucine tRNA isoacceptors on ribosome occupancy at leucine codons during leucine starvation.

(B and E) Mean ribosome occupancy as a function of serylation rate for the six serine codons calculated from whole-cell model. In the differential serylation case (D), the serylation rate constants were in the proportion 0.5: 0.5: 1.5: 1 (Ser1, Ser2, Ser3, Ser5). See also Figures 3C, 3D.

(F and G) Leucine starvation in yeast was simulated using the model of (Shah et al., 2013). In (F), the total concentration of leucine tRNA isoacceptors was reduced by the indicated amount (1 indicates nutrient-rich growth). In (G), the concentration of aminoacylated (charged) leucine tRNA was reduced while keeping the total concentration fixed.

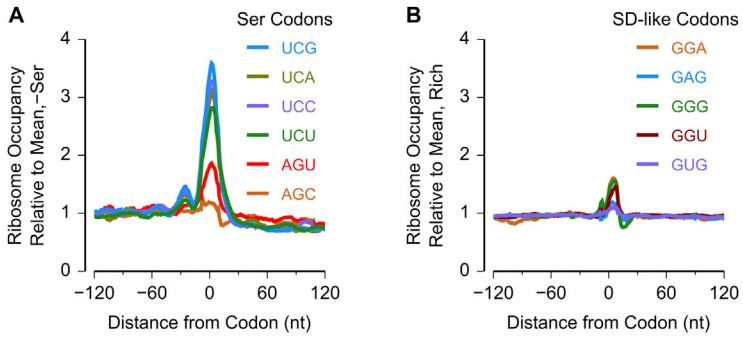

Figure S3. Ribosome Occupancy around Serine Codons and Shine-Dalgarno-like Codons, Related to Figure 4

(A) Measured ribosome occupancy averaged across the transcriptome from −120 nt to +120 nt around the six serine codons during serine starvation.

(B) Measured ribosome occupancy averaged across the transcriptome from −120 nt to +120 nt around five Shine-Dalgarno like codons during nutrient-rich growth.

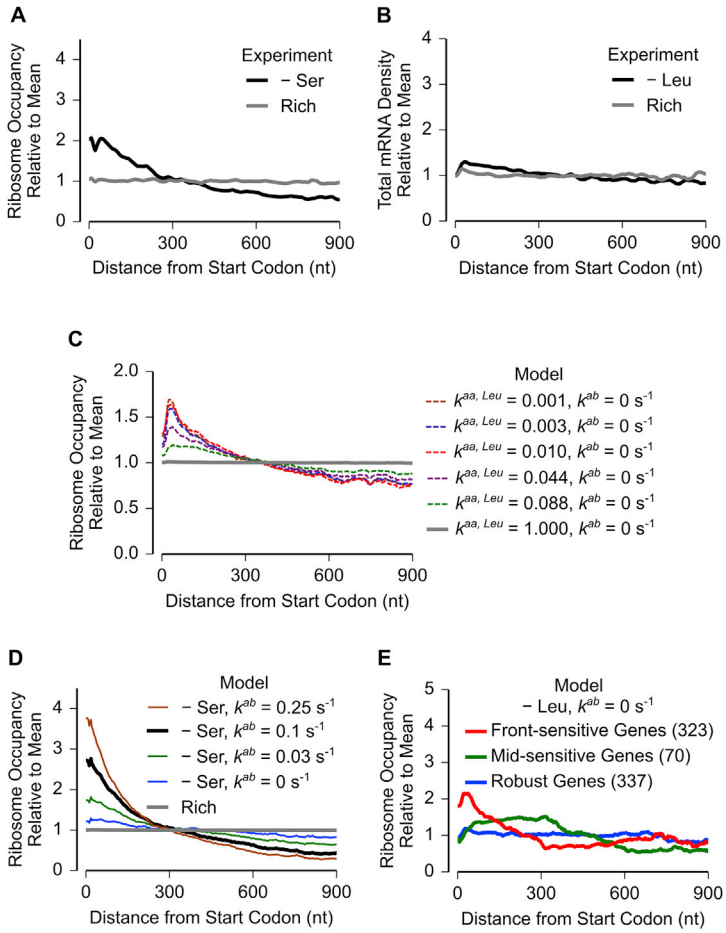

Figure S4. Effect of Varying Aminoacylation Rate and Abortion Rate on Ribosome Occupancy along mRNAs, Related to Figure 5

(A) Measured ribosome occupancy along mRNAs averaged across the transcriptome (1518 genes) during serine starvation and nutrient-rich growth.

(B) Measured mRNA read density averaged across the transcriptome during leucine starvation and during nutrient-rich growth.

(C) Ribosome occupancy along mRNAs averaged across the transcriptome (1518 genes) calculated from the whole cell model with a constant abortion rate (k^{ab}) of 0 s^{-1}. The leucylation rate constant k^{aa} was varied, and a relative value of 1 corresponds to nutrient-rich growth. All other model parameters are as in Table S1.

(D) Ribosome occupancy along mRNAs averaged across the transcriptome (1518 genes) during serine starvation calculated from the whole cell model. The abortion rate constant k^{ab} was varied. Serine starvation was modeled by a 100-fold reduction in serylation rate. All other model parameters are as in Table S1.

(E) Ribosome occupancy averaged across the three sets of genes during leucine starvation calculated from whole cell model with zero abortion rate (k^{ab}). The intragenic distribution of CTA, CTC and CTT codons in the three sets of genes is shown in Figure 5C.

Ribosome occupancy profiles in all panels were smoothed using a sliding window of 30nt. Each ribosome occupancy profile was normalized to have a mean value of 1.

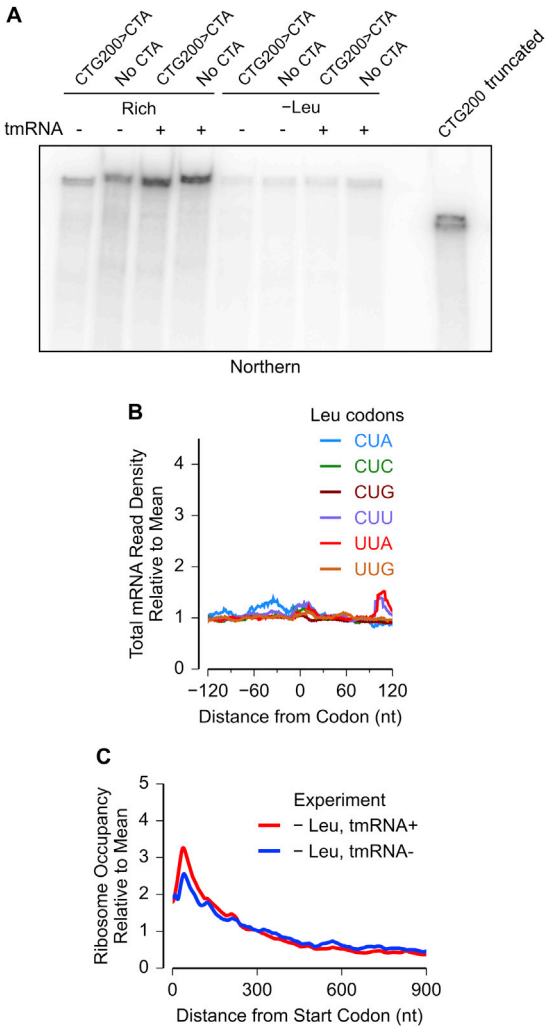

Figure S5. Effect of Abortion on Total mRNA Density, Ribosome Occupancy, and Protein Expression, Related to Figure 6

(A) Northern Blot against total mRNA from strains expressing the three *yfp* reporter variants shown in Figure 4C. The *yfp* reporter variants were induced for 30 min during nutrient-rich growth or during leucine starvation in *tmRNA+* or *ΔtmRNA* strains. The 300nt, P^{32}-labeled, anti-sense RNA probe shown in Figure 4C was used for detecting the *yfp* reporter mRNAs.

(B) Measured total mRNA read density from −120 nt to +120 nt around the six leucine codons during leucine starvation. The read density was averaged across all occurrences of each codon in the transcriptome.

(C) Measured ribosome occupancy along mRNAs averaged across the transcriptome for wild-type (*tmRNA+*) and *ΔtmRNA* strains. Ribosome occupancy profiles were smoothed using a sliding window of 30 nt.

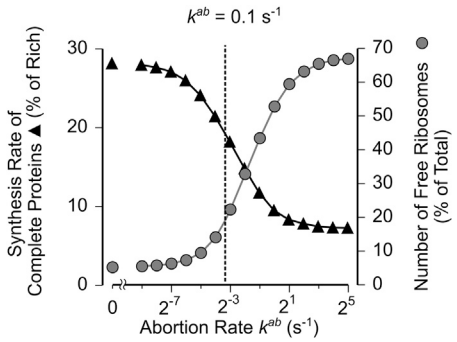

Figure S6. Effect of Abortion on Protein Expression during Serine Starvation, Related to Figure 7

Effect of varying the abortion rate constant (k^{ab}) on the number of free ribosomes in the cell (circles) and the global synthesis rate of complete proteins (triangles) during serine starvation calculated from our whole-cell model. The value k^{ab} = 0.1 s^{-1} which fits the measured ribosome density profile (black line in Figure S4C) is indicated as a dashed line. All other model parameters are shown in Table S1.